Master of Science Thesis
VT-2018

Natural Sugar as an MRI Contrast Agent for Brain Cancer Detection Using Chemical Exchange Saturation Transfer (CEST) Imaging at 3 T

Anina Seidemo

Supervisors:
Linda Knutsson
Anna Rydhög

Department of Medical Radiation Physics,
Clinical Sciences, Lund
Lund University
www.msf.lu.se

Abstract

Background and Purpose: Dynamic glucose-enhanced (DGE) imaging is a novel technique that can be used to assess information about microvasculature by using natural sugar (D-glucose) as a biodegradable contrast agent. The method relies on chemical exchange saturation transfer (CEST). The hydroxyl protons in glucose are saturated using a selective radio-frequency pulse and will subsequently exchange with non-saturated water protons. This approach, called glucoCEST, will lower the water signal so that the presence of glucose can be studied through its saturation effect on the water signal. DGE is an approach in which glucoCEST is applied dynamically to track glucose response over time. Earlier studies (1-4) have successfully shown that glucoCEST and DGE can be used for tumor imaging at higher field strengths and the translation to clinical field strengths (3 T) is ongoing.

The aim of this master thesis project was to implement glucoCEST at 3 T and to compare dynamic response curves in arteries, so called arterial input functions (AIFs), to blood glucose levels sampled over the same time period. A secondary goal was to compare DGE images from this study with DGE images from a 7 T-study.

Materials and Methods: 3 healthy volunteers and 2 patients were scanned on a 3 T scanner (Siemens Prisma) and 50 mL D-glucose (50% dextrose) were manually administered intravenously after 3 minutes of imaging. The infusion duration was approximately 1 minute and the total scan time was 15 minutes. To acquire glucoCEST images, RF-pulses were applied at a saturation offset of 2 ppm. A single axial slice of the brain was imaged dynamically using a single-shot turbo gradient echo. Blood samples were collected at predefined time points to enable monitoring of blood glucose levels as a function of time following the glucose infusion. DGE images were created by calculating the signal difference between each dynamic image and the averaged pre-infusion image. Dynamic response curves were calculated in chosen regions of interest (ROIs) in an artery and in white matter and were compared to blood glucose curves.

Results and Discussion: The DGE images acquired at 3 T showed a change in the water signal after glucose infusion in all subjects. The signal change in a cerebral artery, which was attributed to the altered glucose concentration, did generally correspond to the change in blood glucose level in a peripheral vein. Enhancement of the tumor region was seen in one patient. Each subject showed an individual response to the glucose infusion, addressed to the variance in metabolism and insulin response between subjects. GlucoCEST at 7 T had a higher specificity, but the results indicate that the method works well also at 3 T.

Conclusion: The results showed that glucoCEST and DGE contrast is feasible at 3 T. The study indicates that tumor enhancement is possible, but due to the low number of participants (3 healthy volunteers, 2 patients) the project should be continued by scanning more patients and optimizing the method further. Possible improvements to the method could be to improve the CEST-sequence, by for example extend the saturation duration and include CSF suppression, and to implement a kinetic model for calculation of perfusion parameters.

Användning av socker som kontrastmedel för diagnostisering av hjärncancer med magnetkamera

Hjärntumörer utgör cirka 2,5% av alla cancerdiagnoser i Sverige (2013) och femårsöverlevnaden är cirka 50% (5). Hjärntumörer diagnostiseras med bildtagningstekniker såsom datortomografi (CT), positronemissionstomografi (PET) och magnetkamera (MR). En MR-bild byggs upp av signaler från protoner i vatten, som är en av människokroppens vanligaste beståndsdelar. För att möjliggöra diagnostisering och klassificering av tumörer används ett kontrastmedel som sprutas in i blodet, och på så vis kan information om blodflödet i hjärnan och framförallt i tumören erhållas. De MR-kontrastmedel som används är i regel väldigt säkra men kan påverka vissa patientgrupper negativt och på senare år har det påvisats att de kan ansamlas i vissa vävnader efter upprepade undersökningar (6-9). Metoden begränsas även av att inte alla tumörer tar upp kontrastmedlet (10).

Nackdelarna med den nuvarande metoden skapar ett behov av en ny typ av kontrastmedel. CEST (Chemical Exchange Saturation Transfer) är en teknik som innebär att små mängder av ett ämne kan detekteras med magnetkamera. CEST-tekniken öppnar upp för användning av andra typer av kontrastmedel, exempelvis kan kroppsegna ämnen, såsom vissa proteiner som är vanliga i tumörer, detekteras. Dessutom kan vanligt socker (glukos) injiceras och användas som kontrastmedel, en teknik som kallas för glucoCEST. Socker är väl lämpat för användning som kontrastmedel, dels eftersom det är en naturlig del av vår kost, men också för att tumörer ofta har ett ökat energibehov. GlucoCEST-tekniken bygger på att protoner i sockret märks magnetiskt med en radiofrekvent puls. Därefter sker ett utbyte mellan de märkta protonerna och omärkta protoner i fritt vatten vilket leder till att MR-signalen ändras där glukos är närvarande. Genom att injicera glukos intravenöst samtidigt som patienten ligger i kameran kan en bild som ger information om blodflödet i hjärnan skapas.

I det här projektet implementeras glucoCEST-tekniken på en magnetkamera i kliniskt bruk, vilket inte har gjorts tidigare i Sverige. Både friska frivilliga och patienter med hjärntumör deltog i studien. Genom att analysera blodprover som tas kontinuerligt under undersökningen kan blodsockervärdet jämföras med den ändring i MR-signalen som fås då sockret sprutas in och når hjärnan. Resultaten jämförs med data från ett forskningsprojekt utfört vid en magnetkamera med högre magnetfält.

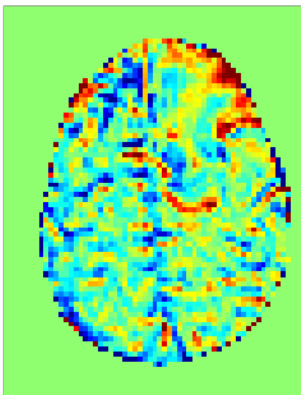

Exempel på en bild skapad med hjälp av gluco-CEST-teknik i en patient med hjärntumör.

En ändring av MR-signalen, som generellt sett följde ändringen av blodglukosnivån, kunde ses i alla deltagare (framförallt i blodkärl), men det är ännu inte helt klart vilka fysiologiska parametrar som kan extraheras ur glucoCEST-bilderna. Resultatet av studien indikerar att glucoCEST har potential att bli ett alternativ eller komplement till konventionella kontrastmedel, även om mycket arbete kvarstår. Sammanfattningsvis har det här projektet tagit ett första steg mot klinisk implementering av glucoCEST-tekniken.

List of abbreviations

ACA - Anterior cerebral artery
AIF - Arterial input function
APT - Amide proton transfer
AUC - Area under curve
BBB - Blood-brain barrier
CEST - Chemical exchange saturation transfer
CNS - Central nervous system
CSF - Cerebrospinal fluid
DCE - Dynamic contrast enhanced
DGE - Dynamic glucose-enhanced
DS - Direct water saturation
EES - Extravascular extracellular space
FA - Flip angle
GBCA - Gadolinium-based contrast agents
Gd - Gadolinium
GRE - Gradient echo
MRI - Magnetic resonance imaging
MT - Magnetization transfer
MTC - Magnetization transfer contrast
NMR - Nuclear magnetic resonance
NOE - Nuclear Overhauser enhancement
NSF - Nephrogenic systemic fibrosis
PTR - Proton transfer ratio
PVE - Partial volume effects
ROI - Region of interest
SAR - Specific absorption rate
SNR - Signal-to-noise ratio
TE - Echo time
TR - Repetition time
WM - White matter

Table of contents

1 Introduction

Brain cancers make up around 2.5% of all cancer diagnoses in Sweden and the five-year survival is approximately 50% (5). Brain tumors are treated primarily by surgery, and sometimes with adjuvant chemo- and radiotherapy. Modern imaging modalities such as computed tomography (CT), magnetic resonance imaging (MRI) and positron emission tomography (PET) are used for the diagnosis of brain cancer. Examinations made on these modalities require a radioactive (in PET) or potentially toxic (in CT and MRI) contrast agent to be administered. One example is perfusion MRI, where a contrast agent is administered intravenously during the examination. The signal change over time caused by the passage of the contrast agent can then be used to assess information about blood flow, blood volume and permeability of the blood-brain barrier (BBB). The clinical contrast agents for MRI used today are generally very safe but have occasionally caused adverse effects in some patient groups and have been found to accumulate in tissues after repeated use (6-9). Conventional MRI contrast agent methods are also restricted by the fact that not all tumors are contrast-enhancing (10).

For these reasons, the implementation of new types of contrast agents is attractive. Chemical exchange saturation transfer (CEST) MRI is a technique in which small amounts of a compound can be detected. CEST combines the molecular specificity of magnetic resonance spectroscopy (MRS) with the sensitivity of MRI and provides the possibility of using endogen substances as contrast agents, such as proteins that are common in tumors. Natural sugar (D-glucose) can be utilized in a CEST-technique called glucoCEST (4, 11). The principle of glucoCEST is that protons in the hydroxyl groups in glucose are magnetically labelled by a radio-frequent pulse, followed by an exchange between the labelled protons and the non-labelled protons in free water. This causes a change in the MR signal that is proportional to the concentration of the compound in a tissue or vessel. The signal change can give information about blood volume and permeability in the brain. The advantages of sugar as a contrast agent are obvious, being a well-known part of our diet, and it is already in clinical use for glucose tolerance testing (used in diabetes investigations). Tumors are known to have a high glucose consumption and sugar is also used as a tumor-enhancing contrast agent in PET, with radioactively labelled glucose. An advantage of glucoCEST (over other imaging modalities) is that it is a radiation-free alternative and that MRI can provide supplementary high quality anatomical images.

GlucoCEST is not yet clinically implemented but has shown promising results in studies of both animals (3) and humans (2). Since CEST benefits from higher field strengths, most studies have been performed at 7 Tesla (T) or higher, but the clinical availability to such high field strengths is limited. Therefore, the aim of this study is to implement glucoCEST at 3 T (for the first time in Sweden). The study includes both healthy volunteers and patients with brain tumors. Intravenous administration of glucose during dynamic

glucoCEST imaging causes a change in the MR signal over time. This approach is called dynamic glucose enhanced (DGE) MRI (2, 3). By taking blood samples during the scan, the blood glucose level can be compared to the DGE signal in different regions of the brain. The signal change in a cerebral artery can be interpreted as an arterial input function.

Aims

- To apply glucoCEST in patients with brain cancer and healthy volunteers at 3 T, and to compare this with glucoCEST at 7 T

- To compare arterial input functions from glucoCEST acquired at 3 T and 7 T with blood glucose levels

- To compare the image quality in glucoCEST collected at 3 T and 7 T

2 Theory

Clinical magnetic resonance imaging (MRI) uses information from hydrogen nuclei, which is abundant in human tissue. MRI contrast originates from the physical properties of the tissue, which causes different relaxation times in different tissues. A contrast agent can be used to increase the sensitivity or specificity in imaging by altering the relaxation locally in for example a tumor.

2.1 MRI contrast agents

Contrast agents are used to improve images and provide physiological and anatomical information that is not attainable with conventional imaging. The contrast agent is administered into the blood stream and when combined with imaging, information about perfusion properties of tumors such as permeability, blood flow and blood volume can be determined. The parameters that can be obtained depend on which method and contrast agent that is used.

The most frequently used contrast agent in MRI is based on gadolinium (Gd), which is a rare earth metal. The adequacy of Gd as a contrast agent for MRI originates from its electronic structure which causes its strong paramagnetic properties. Gd affects the relaxation in adjacent water protons via dipole-dipole interactions between the electrons in Gd and the water protons in tissues where it is deposited. The relaxivity varies between different types of gadolinium-based contrast agents (GBCAs) and the relaxation rate increases as a function of Gd concentration. A shortening of T_1 is achieved where the Gd concentration is higher than its surroundings, causing a higher signal in the T_1-weighted image.

Gd is administrated intravenously (or orally for gastrointestinal tract exams). Because of the toxicity of free Gd it needs to be chelated to a ligand before being used as a contrast agent. Chelated Gd cannot penetrate the blood brain barrier (BBB) but will cross over where the BBB is damaged. The GBCA is excreted through the kidneys with a biological half-life of around 2 hours (12) in patients with normal renal function. Chelation reduces the acute toxicity and increases the excretion rate of the contrast agent and the stability of a GBCA depends on the chemical structure of the chelating agent. Linear agents have a higher probability of releasing the gadolinium and are therefore considered less safe than macrocyclics (8, 13-16).

A disadvantage of GBCA is that dissociated Gd deposited in tissue has been linked to nephrogenic systemic fibrosis (NSF), a severe disease that can occur in patients with renal impairment (12, 17). In addition, accumulation of gadolinium in deep brain nuclei and in bone has been found in patients with normal kidney function who have undergone several MRI examinations with GBCAs (6, 7, 9, 15, 16, 18). This has also been verified in a rat model (8) and is primarily connected to linear agents. On account of this, some linear

intravenous gadolinium agents were suspended in 2017 by the EMA (European Medicines Agency) (19), and FDA (U.S. Food & Drug Administration) issued a warning regarding the use of GBCA (20). EMA recommends that gadolinium contrast agents should only be used when required diagnostic information cannot be obtained without contrast enhancement and that the lowest possible dose which provides sufficient image enhancement for diagnosis should always be used (19). FDA and ISMRM (International Society of Magnetic Resonance in Medicine) give similar recommendations (20, 21). In spite of this, GBCAs are still essential in diagnosing some life-threatening conditions and should be used when necessary. GBCAs are contraindicated in patients with renal malfunction and special caution should be taken regarding the use in pregnant women, children and patients with inflammatory diseases.

At present there is no evidence that brain deposition of gadolinium is associated with any adverse behavioral or neurological effects. Still, these warnings might worry patients and cause some individuals to refuse important examinations when Gd injections are needed. The drawbacks of gadolinium-based contrast agents increase the need for a new type of contrast agent for MRI and one promising approach might be CEST MRI.

2.2 The CEST-mechanism

CEST MRI is a technique that offers a new type of molecule specific MRI contrast. CEST imaging provides the possibility of using endogen compounds as contrast agents and is a promising alternative to the use of invasive contrast agents such as Gd.

CEST relies on the fact that protons in a compound, for example a metabolite or a contrast agent, has a particular resonance frequency different from the water proton resonance frequency. This particular frequency can be expressed as a chemical shift with respect to the water resonance frequency. The compound, often referred to as a solute, has a low concentration (typically μM or mM) in the body compared to water and is thus not distinguishable from the ordinary MR signal originating from water protons with a concentration around 110 M (22). The protons in the solute can be selectively saturated using a radio-frequent (RF) pulse corresponding to the specific resonance frequency (saturation means equilibrium between the two spin states causing a zero net magnetization vector). If the protons in the solute are exchangeable the saturation can be transferred to water protons via chemical exchange, which will cause a modest reduction of the water signal. This effect will increase if the process is repeated, resulting in a buildup of saturation in water.

The process can be described by a two-pool model with one pool representing the solute protons and a much larger pool representing the water protons. The resonance frequency will differ between the two pools as a result of their different chemical and physical environment. After the RF-saturation, the saturated solute protons will physically change place with unsaturated protons from the water pool. This process will be repeated as long as the

RF-pulse is present, causing a considerable fraction of the water protons to be saturated and thus leading to a measurable reduction of the water signal and an increased image contrast between tissues. The concept is illustrated in figure 2.1.

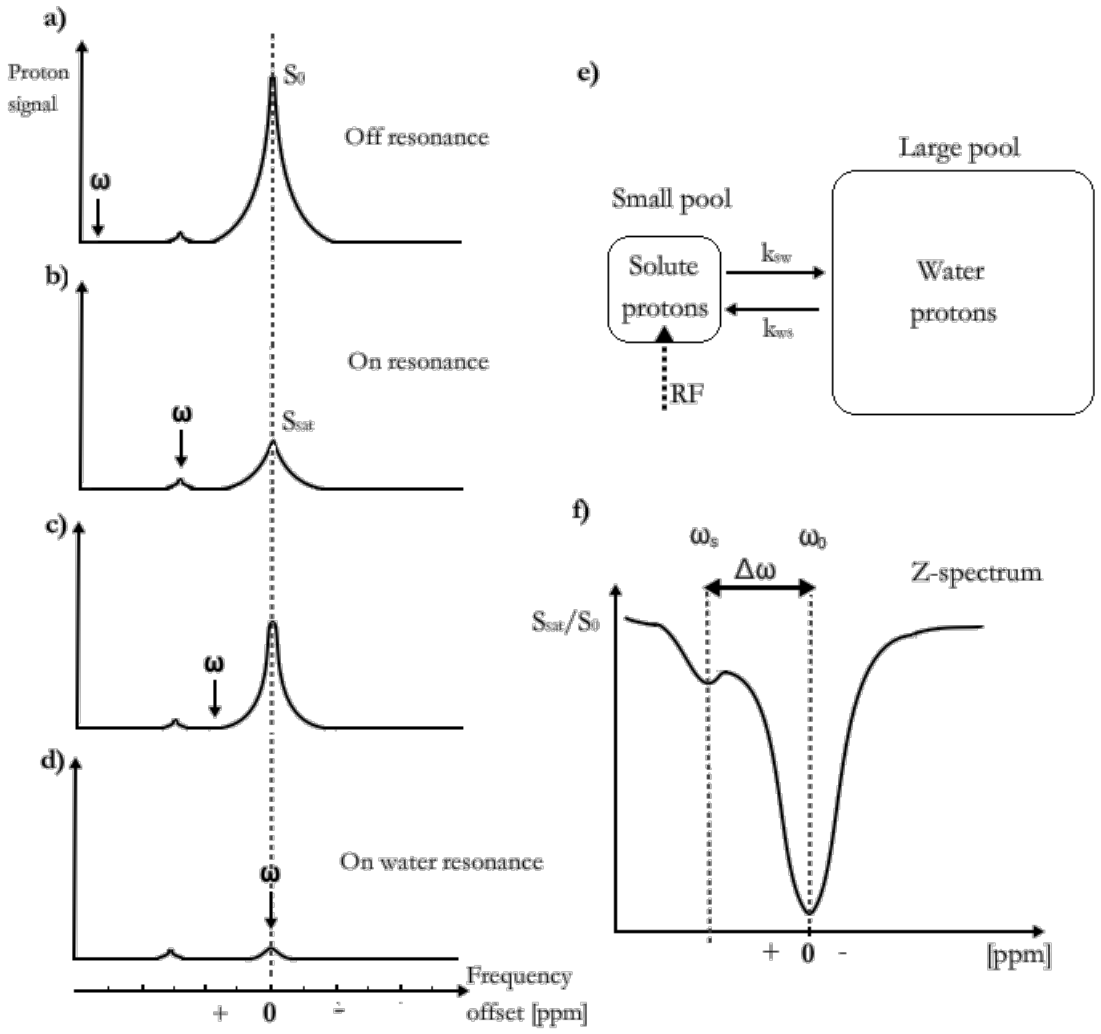

Figure 2.1. When an off-resonance frequency is used, as shown in **a)**, the water signal is much larger than the solute signal. When an RF-pulse is applied on the solute resonance frequency ω_s, the water signal is attenuated as in **b)**, because of saturation transfer. If the applied frequency ω is in between ω_s and the water resonance frequency ω_0, showed in **c)**, the effect on the water signal S_0 is smaller than in **b)**. When $\omega = \omega_0$ the water signal disappears, shown in **d)**. The saturation exchange between the two pools are schematically described in **e)**, where k_{sw} and k_{ws} is the exchange rate from solute to water and from water to solute, respectively. A so-called Z-spectrum, **f)**, is achieved by normalizing the saturated signal S_{sat} for an interval of frequencies to the unsaturated signal S_0 and present it as a function of RF-frequency. The Z-spectrum is used for measuring and analyzing the CEST-effect, as described in a later section.

In reality, the RF-pulse is not perfect (it does not only target the exact required frequency) and a solute resonance frequency close to the water frequency will increase the contribution from direct water saturation (DS), as depicted in figure 2.1 d).

The saturation exchange process is strongly dependent on the exchange rate ratio between the two pools. The CEST-effect increases with the exchange rate from the solute to the water k_{sw}, but it should not be too large since the solute protons needs to be sufficiently saturated before the exchange takes place. It is also important that the chemical shift is large enough to allow for selective saturation of the solute protons (minimizing the DS effects). Altogether, this implies that the exchange rate must be in the slow to intermediate range on the NMR time scale (23):

$$\Delta\omega_{\mathrm{sw}} \geq k_{\mathrm{sw}}, \tag{2.1}$$

where ω_{sw} is the chemical shift, i.e. the difference in resonance frequency between solute and water protons in radians/second.

The theory behind the CEST mechanism is described by the Bloch-McConnell equations (24), which are based on modifications of the Bloch equations with the purpose to incorporate the kinetic processes of magnetization transfer between two pools. By assuming a slow exchange rate in a two-pool model with no back-exchange or DS of the water protons, the analytical solution to the Bloch-McConnell becomes equation 2.2 (see for example (25)). This is the proton transfer ratio, PTR, describing the CEST-effect under these assumptions:

$$\mathrm{PTR} = x_{\mathrm{s}} \cdot \alpha \cdot k_{\mathrm{sw}} \cdot T_{1\mathrm{w}} \cdot \left(1 - e^{t_{\mathrm{sat}}/T_{1\mathrm{w}}}\right), \tag{2.2}$$

where x_{s} is the fraction of solute protons with respect to the water proton concentration, α is the saturation efficiency of the solute proton pool, k_{sw} is the exchange rate from solute to water, $T_{1\mathrm{w}}$ is the T_1 relaxation time for water and t_{sat} is the saturation duration time. The saturation efficiency, α, depends on the applied RF-field (B_1) and on the exchange rate k_{sw}.

From equation 2.2 it is clear that the PTR is proportional to the concentration of exchangeable solute protons and to the exchange rate from solute to water. The PTR, and then also the CEST-effect, increases with magnetic field strength because a higher field strength implicates a larger chemical shift and a longer T_1 of water. A longer T_1 will cause the saturation to last longer, which is beneficial for the CEST-effect. A higher field strength will therefore allow compounds with a higher exchange rate, in accordance with equation 2.1, which is beneficial for the CEST-effect.

PTR is also sensitive to pH and temperature (26). The exchange rate increases with increasing pH and a higher CEST-effect can be detected as long as the exchange rate remains in the slow to intermediate range. It is possible to take advantage of the pH-dependence of CEST imaging since pH decreases in vivo in physiological conditions such as ischemia (27, 28), which therefore yields a lower CEST-effect.

Saturation transfer via chemical exchange is not the only saturation transfer pathway and other processes than CEST will influence the result (the image and the Z-spectrum). The relaxation of a saturated system will not depend entirely on the exchanged protons, the saturation is also transferred between spin systems. The two principal mechanisms for saturation transfer are cross-relaxation through dipolar coupling and chemical exchange. The main difference is that in the first case only the saturation is transferred but in the second case the saturated proton is physically changing place. The next section will give a brief introduction to different kinds of magnetization transfer (MT).

2.2.1 Magnetization transfer processes

A saturated or excited spin pool can influence signal intensity in an adjacent spin pool due to cross-relaxation. Saturation or magnetization can be transferred from one spin system to another via intra- or intermolecular dipolar interactions. The extent of this effect depends on the distance and the coupling between the protons and it increases with reduced molecular rotational motion. This change in signal intensity due to cross-relaxation is called a NOE (nuclear Overhauser enhancement). The saturation transfer can be relayed through the molecule, which is called spin diffusion. NOE is more prominent in immobile macromolecules (as in semi-solid tissues) than in smaller rapidly moving molecules, such as free water.

Transfer of NOEs between protons is referred to as relayed NOE (rNOE). The process where the saturation initially is transferred to a molecule via chemical exchange, followed by spin diffusion spreading through the molecule, is called exchange-relayed NOE. If the course of events is reversed, i.e. the proton gets saturated and relayed via spin diffusion within the molecule followed by an exchange with a proton in another molecule, the process is called NOE-relayed exchange. These different processes are illustrated schematically in figure 2.2.

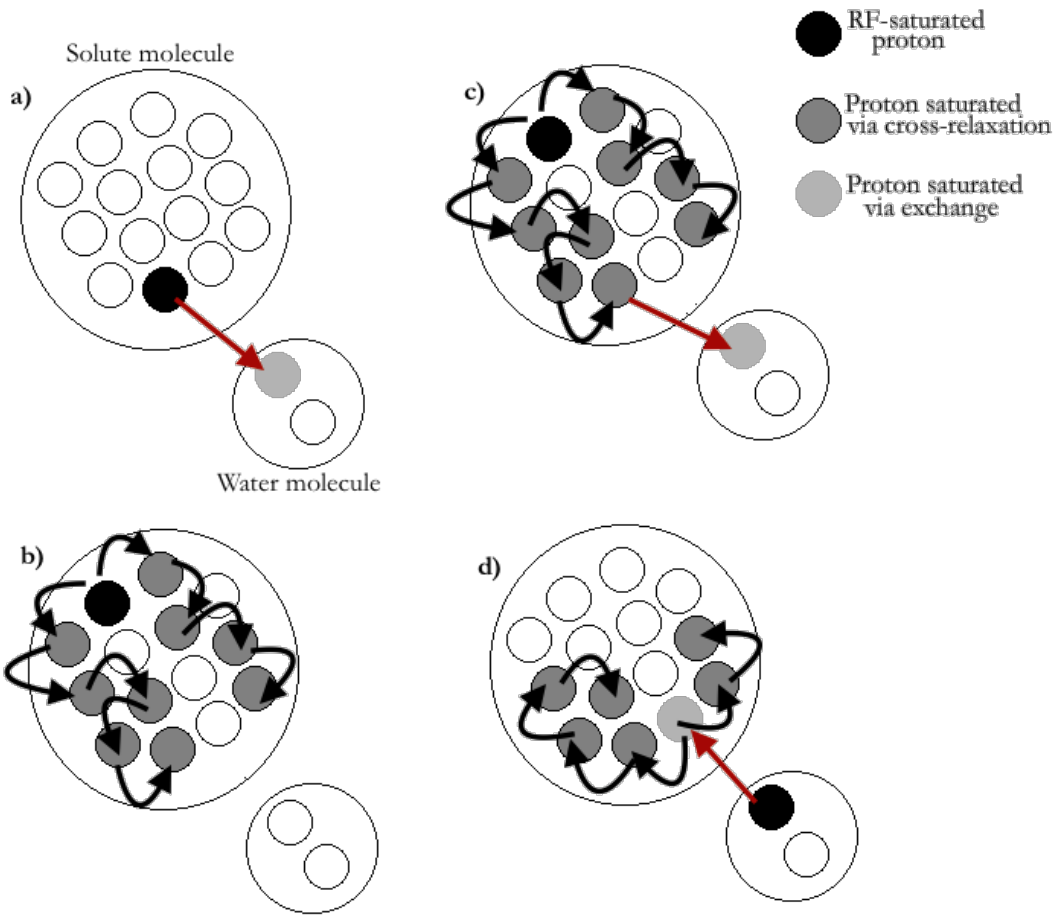

Figure 2.2. A simplified illustration of different saturation transfer processes. The solute molecules are represented as circles with H-protons inside (other atoms are excluded in this example, but these H-protons are parts of for example NH- or OH-groups in a larger molecule). Water molecules are represented as smaller circles including two H-protons. Chemical exchange is pictured in **a)**, where the (red) straight arrow represent the two protons switching places. The process illustrated in **b)** is spin diffusion; the saturation is transferred from an RF-saturated proton to neighboring protons through NOEs, indicated with curved arrows. **c)** and **d)** represent NOE-relayed exchange and exchange-relayed NOE respectively.

An off-resonance RF-pulse leads to partial saturation of protons with large dipolar coupling in immobile semi-solid macromolecules followed by magnetization transfer and a reduction of the water signal. The saturation will in this case not affect mobile molecules and the approach can be used to generate images with magnetization transfer contrast (MTC). The main difference between MTC and CEST is that the former dominates in semi-solid tissue, and the latter for mobile molecules.

In summary, the CEST signal will include contributions from all these saturation transfer effects, making the image interpretation more complex. It is therefore important to be

familiar with these effects when analyzing experimental results (29).

2.2.2 The Z-spectrum

A Z-spectrum can be acquired by collecting images with frequencies in an interval around the water frequency and then normalizing the saturated water signal intensity $S_{sat}(\omega)$ to the non-saturated signal S_0 and present that ratio as a function of frequency. An example of a Z-spectrum was shown in figure 2.1 f) and the features of the Z-spectrum can be understood by studying figure 2.1 a-d). The water resonance frequency is in this context assigned to the value zero and the other frequencies can then be expressed in ppm (parts per million) relative to the water frequency. In this manner the frequency can be specified regardless of the field strength. Negative frequencies are placed to the right (upfield) and positive frequencies to the left (downfield) in the spectrum.

The Z-spectrum includes contributions from all types of MT (CEST, NOE and MTC) and the proportion of each component is dependent on B_0, the strength of B_1 (the RF-power) and the tissue, which it is originating from. It is thus complicated to determine the relative contribution from each MT process. The reduction of the water signal will be both due to chemical exchange and to other MT effects. The contribution from direct water saturation, which can be assumed to manifest symmetrical around the water resonance frequency in the Z-spectrum, can be removed through symmetry analysis. One way to do this is to calculate MTR_{asym}, a parameter that represents the asymmetry of the Z-spectrum caused by the exchanged protons:

$$\mathrm{MTR_{asym}} = \mathrm{MTR}(\Delta\omega) - \mathrm{MTR}(-\Delta\omega) = \frac{S_{\mathrm{sat}(-\Delta\omega)} - S_{\mathrm{sat}(\Delta\omega)}}{S_0} \tag{2.3}$$

As seen in equation 2.3, MTR_{asym} is the difference in signal at one frequency and the signal at the corresponding frequency on the opposite side of the Z-spectrum, normalized to the unsaturated signal. Other MT effects than DS are not necessarily symmetric around the water frequency. NOE signals will for example be found on the negative side of the Z-spectrum. MTCs are slightly asymmetric and present throughout the entire Z-spectrum, and the relative MTC-contribution increases with increased RF-power. The shape of the Z-spectrum can give information about the environment in the tissue it is originating from. Changed tissue properties, in for example ischemia or tumors, will affect the type of magnetization transfer in the tissue, and therefore also the Z-spectrum and the PTR (27, 30).

2.3 Pulse sequences for CEST imaging

A typical CEST MRI pulse sequence includes one saturation part and one imaging part. In the saturation part, a long (typically a couple of seconds) RF pulse is applied. As seen in equation 2.2, the CEST-effect will increase with the time duration of the RF pulse. Increased RF-power implies more direct saturation of the water pool as well as a larger MTC contribution. It will also be limited by RF hardware and by specific absorption rate (SAR)

in vivo. Saturation can be achieved by using a continuous wave RF pulse or a pulse-train (series of saturation pulses separated by short (in the order of a few milliseconds) time intervals). Because of the reasons mentioned above, pulsed saturation is preferable for clinical CEST imaging. Each saturation block is followed by a rapid image acquisition sequence.

2.4 CEST applications

Both paramagnetic and diamagnetic contrast agents can be utilized for CEST imaging, giving rise to the terms diaCEST and paraCEST. ParaCEST agents have a larger chemical shift but are less attractive as a contrast agent since they include metallic ions and are potentially toxic. The focus of this section is therefore on diaCEST agents.

In theory, almost any compound including a chemical group with exchangeable H-protons is suitable for CEST imaging. The ideal CEST contrast agent has a large chemical shift and must obey equation 2.1 (the exchange rate has to be smaller than, or equal to, the chemical shift) and for imaging in humans it needs to be an endogenous or non-toxic exogenous substance. A number of chemical groups and their suitability for CEST imaging were evaluated by Ward et al. in 1999 (23), regarding chemical shift and exchange rate at physiologic pH and temperature.

Chemical groups with exchangeable protons generally have frequencies higher than the water proton resonance frequency, and they are found on the positive side of the Z-spectrum (downfield from water). Examples of such aromatic groups are hydroxyl (-OH), amide (-NH) and amine ($-NH_2$), having chemical shifts in the order of 0-3.5, 3.5 and 2-3 ppm respectively (29). APTw (amide proton transfer-weighted MRI) detects amide protons of mobile proteins and peptides present at a higher concentration in cancer tumors. APTw can also be used for imaging of ischemic stroke because of the reduction of pH, implicating a reduction in proton exchange rate (27, 28).

Other CEST applications are imaging of for example glycosaminoglycan (gagCEST) in cartilage that can be used as an indicator for osteoarthritis (31, 32), glutamate (gluCEST) in the CNS (in Alzheimer's diagnostics) (33, 34), and glycogen (glycoCEST) in metabolism studies (11). The approach targeted in this project is glucoCEST, where natural D-glucose is administered intravenously as a biodegradable contrast agent to gain information about cerebral perfusion and glucose uptake in tumors. The glucose molecule has five hydroxyl groups, three of them resonate around 1.2 ppm and the other two at 2.1 and 2.9 ppm from water respectively (4, 26).

2.5 Glucose metabolism

Glucose is a monosaccharide consisting of six carbon atoms (a hexose), with the molecular formula $C_6H_{12}O_6$. The glucose uptake and metabolism in the cell takes place in the cytosol (the intracellular fluid) through anaerobic metabolism via glycolysis, and in the mitochondria where the process is aerobic. Glycolysis is a sequential pathway for conversion of glucose into pyruvate and a large amount of ATP (energy) is rapidly produced. Excess blood glucose is stored in the form of glycogen in skeletal muscles and to some extent in the liver. The rest is converted to fat. The liver plays an important role in maintaining a constant blood glucose level, through both glycogenolysis (breakdown of glycogen into glucose) and glyconeogenesis (generation of glucose from non-carbohydrates). Normal fasting blood glucose levels are 3.9 to 6.1 mmol/L (70 to 110 mg/dL) (35).

The blood glucose level is regulated through interplay between primarily two hormones: glucagon and insulin. These hormones are synthesized by alpha and beta cells, respectively, in the islets of Langerhans belonging to the endocrine pancreas. Insulin has a hypoglycemic effect - it reduces blood glucose levels by stimulating glucose uptake in peripheral tissues (mainly muscular and fat tissue) and through activation of transport mechanisms in the cell membrane. At hyperglycemia (high blood glucose levels) the secretion of insulin is increased, leading to a higher glucose uptake in the cells and therefore an increase of glucose conversion into glycogen. The insulin also prevents glycogenolysis in the liver. These two insulin dependent factors will together result in a lower blood glucose level. Hypoglycemia (low blood glucose levels) will instead reduce the insulin secretion and amplify the secretion of glucagon, which will lead to stimulation of glycogenolysis causing an increase in blood glucose levels. Insulin is released from pancreas in two phases. The first phase is rapidly initiated (normally within 1-3 minutes (36)) as a response to raised blood glucose levels and lasts for a short time (around ten minutes). The second phase that follows lasts for several hours and is characterized by a slow, extended insulin release.

The brain is fueled primarily by glucose and relies on a constant and well-regulated supply. Glucose reaches the brain via transporter proteins (primarily GLUT1 in BBB and GLUT3 in cell membranes). The transporter proteins in the brain differs from those in peripheral tissues in that they are not insulin dependent. Instead, the glucose influx to the brain depends on the concentration gradient between blood and brain (37).

2.6 Summary

GlucoCEST imaging is a novel technique relying on chemical exchange of saturated protons between a compound (glucose) in low concentration, and water protons, causing a change in water signal intensity where the compound is present. The main goal of this master thesis project is to apply glucoCEST in healthy volunteers and in brain tumor patients at clinical field strength (3 T), and to compare the results to glucoCEST from a former study at higher field strength (7 T).

3 Materials and methods

3.1 Subjects

All data acquisition was performed at Lund University Hospital, and all studies in the project was approved by the local ethics committee (The Regional Ethical Review Board in Lund). Written informed consent was obtained for all subjects. Exclusion criteria were sensitivity for D-glucose (diabetes mellitus, sickle cell disease and blood iron deficiency) and for patients also sensitivity to gadolinium. Creatinine and blood glucose level were measured prior to the examination. When possible, the same volunteers as in the 7 T study were used in the 3 T study. 3 healthy volunteers (1 male and 2 females, age 26-52) and 2 patients (2 male, age 55-76) with brain tumors participated in the 3 T study. The examination was carried out on a 3 T MRI scanner (Siemens Prisma) with a 20-channel head coil (Siemens).

The 7 T data were collected during 2016-present day, using an actively shielded 7 T MRI scanner (Philips Achieva) and a 32-channel phased-array head coil (Nova Medical).

3.2 Data acquisition

All participants were fasting for 4-6 hours before the exam. Fasting is required to stabilize the baseline blood glucose and insulin levels (38). Peripheral venous catheters (PVC) were inserted in both arms. A baseline blood glucose level was measured at arrival to assure a blood glucose level between 3.9-7 mmol/L (70-135 mg/dl).

The 3 T glucoCEST images were collected dynamically (dynamic glucose enhanced MRI) during 15 minutes, giving 134 images with a temporal resolution of 6.7 seconds at saturation offset frequency 2 ppm (247 Hz) from the water frequency. Acquisition of a full Z-spectrum is not needed for dynamic glucose enhanced (DGE) imaging and in order to shorten the scan time, only one saturation offset was used. Non-saturated (S_0) images were acquired at -150 ppm in image number 1, 3, 4, 47, 90, 133 and 134. Saturation was achieved using 5 HypSec pulses with pulse duration 99.8 ms separated by 61 ms interpulse delay. The RF amplitude (B_1) was 2.0 μT. An example of a raw dynamic glucoCEST series, showing one slice of the brain at different time points, is displayed in figure 3.1. GlucoCEST images of one single slice were acquired after each saturation using a gradient echo (GRE). The imaging parameters can be found in table 4.1, together with the corresponding parameters used for acquisition of glucoCEST images at 7 T.

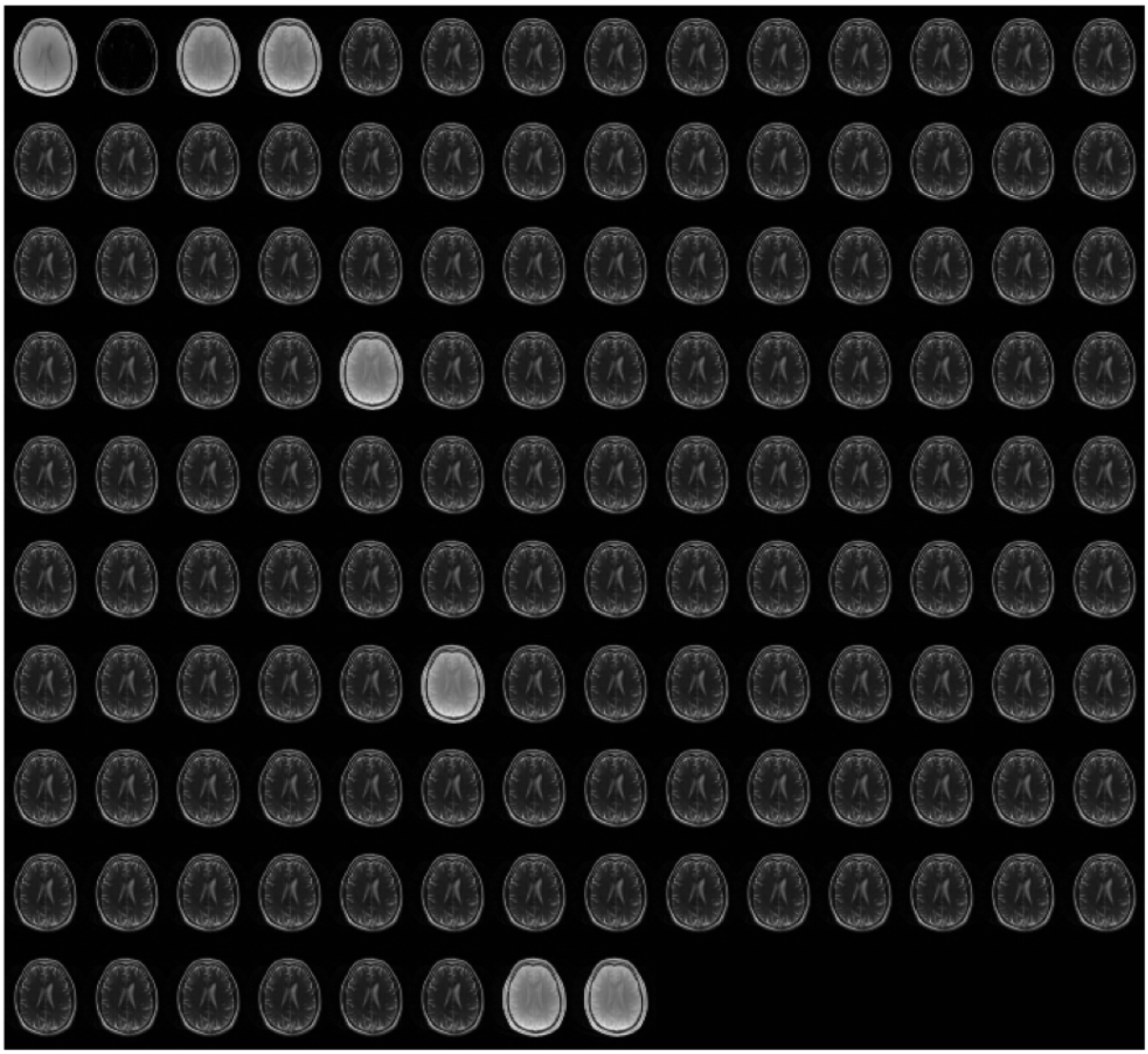

Figure 3.1. Example of raw dynamic CEST images from one healthy volunteer. The temporal resolution is 6.7 seconds. The images with high intensity are the non-saturated S_0 images, and the one dark image (dynamic number two) is saturated at the water resonance frequency (0 ppm). The other images are saturated at 2 ppm, in this case representing the glucose (hydroxyl) resonance frequency.

Table 4.1. Imaging parameters

	3 T Siemens WIP	7 T Philips WIP
Saturation:		
B_1 [**µ**T]	2.0	2.0
Pulse dur/pulse gap/no of pulses [ms/ms/#]	99.8/61/5	50/25/32
Saturation duration [s]	0.5	1.6
Pulse shape	HypSec	Sincgauss
Offset frequency [ppm]	2.0	1.2
Imaging:	single-shot turbo GRE	single-shot turbo GRE
Voxel size [mm^3]	2x2x6	3x3x6
Field of view [mm^2]	256x200	224x224
TR/TE/FA [ms/ms/°]	126/1.96/10	5/1.48/30
Temporal resolution [s]	6.7	5.3
Scan time	15 min	15 min 54 s

50 mL D-glucose (50% dextrose) was manually injected intravenously via plastic tubes in one arm after three minutes of imaging. The infusion time was approximately 60 seconds, ranging between 48 and 78 seconds. In one patient (patient 2) a longer infusion time (127 s) was used. Blood samples (around 1-2 mL per sample) from a vein in the contralateral arm were taken at preset time points. To enable monitoring of the blood glucose concentration, blood samples were analyzed using a blood gas analyzer (i-Stat, Abbot Scandinavia AB). This process was the same at both 3 T and 7 T.

Saturation spectra (Z-spectra) were collected before and after the dynamic scan. The frequency interval ranged from -4 to 4 ppm in steps of 0.25 ppm. The offset frequency for non-saturated images (S_0) were -150 ppm. The scan time for each Z-spectrum was 3 minutes and 45 seconds, and the imaging parameters were the same as for the DGE imaging.

Additionally, Gd-enhanced imaging was included in the examination protocol for patients. 60 T1-weighted dynamic contrast enhanced (DCE) images were collected using TR/TE/FA = 5 ms/1.65 ms/15° during 7 minutes, and a bolus of 0.1 mmol/kg Gd-chelate was injected using an injector. 24 slices were imaged with in-plane resolution 2x2 mm^2, slice thickness 4 mm and field of view 256x256 mm^2.

3.3 Post-processing and data analysis

3 T data were collected during this project, while 7 T data from a former study was used. All data were converted to NIfTI-format and analyzed in Matlab R2017b (MathWorks). A mask of the whole brain was created by the use of a threshold and an erosion-function in order to remove skull and background from the image. To minimize impact of subject movements during the DGE-scan, retrospective image registration was performed using the Elastix (39) software. An affine transform was used, meaning that the images can be translated, rotated, scaled and sheared.

Dynamic glucose enhanced (DGE) images, DGE area under curve (AUC) images and dynamic curves representing the signal change as a function of time were calculated from the dynamic glucoCEST images. Curves describing the venous blood glucose level as a function of time was retrieved from the venous blood samples.

All S_0-images were removed from the glucoCEST image series and the remaining images, all saturated at 2 ppm, were normalized to the third S_0-image. The first two images and the image directly after each S_0-image (which had a higher intensity) were removed from the image series to assure steady-state. The total number of DGE images is therefore 123. A baseline image was calculated as the average of all pre-infusion images (normally 22 images). Each image intensity was then voxel-wise subtracted from S_{base} to create DGE images. A positive value in a voxel will thus represent more reduction of the water signal due to more saturation transfer and therefore a higher glucose concentration. The calculation is described by equation 3.1:

$$\text{DGE} = \frac{S_{\text{base}} - S(t)}{S_0} = \frac{\Delta S}{S_0}, \tag{3.1}$$

where S_0 was chosen as the third non-saturated image. DGE AUC images were calculated as the sum of all DGE images in a given time interval, as described in equation 3.2:

$$\text{AUC} = \sum_{1}^{n} \frac{S_{\text{base}} - S(t_n)}{S_0}, \tag{3.2}$$

where n was chosen so that each AUC image represents a two-minute interval.

The DGE average in chosen regions of interest (ROIs) or selected voxels were calculated and presented as a function of time to create dynamic response curves in which the signal evolution in for example an artery can be studied. 1-3 voxels in the anterior cerebral artery (ACA) were chosen to achieve an AIF. A 3-point moving mean were used to smooth all the dynamic curves.

In order to examine the impact of internal motions such as pulsations, as well as the efficiency of the motion correction, a glucoCEST scan without glucose infusion was performed. A fasting healthy volunteer was instructed to lie as still as possible. DGE AUC maps for two-minute intervals was computed with and without retrospective motion correction using equation 3.2. In this case, all the dynamic images were averaged to form the baseline image S_{base}.

For patients, DCE AUC images (gadolinium-enhanced dynamic area under curve images) were calculated for comparison to DGE AUC, using equation 3.3:

$$\mathrm{AUC}_{\mathrm{DCE}} = \sum_{1}^{n} \frac{S_{\mathrm{base}} - S(t_n)}{S_{\mathrm{base}}}, \tag{3.3}$$

where S_{base} is the average of the pre-gadolinium images. The gadolinium shortens T1 locally within the vessels, and the signal will increase after gadolinium administration. Hence, calculating DCE AUC using equation 3.3 will give a negative voxel intensity where the gadolinium concentration is high, e.g. where the BBB is damaged. The calculated signal was therefore multiplied by -1 to receive an image more intuitively comparable to the DGE AUC images.

The results were evaluated visually. 7 T-data were post-processed using the same Matlab-program and methods as described above.

4 Results

4.1 Healthy volunteers

Three healthy volunteers participated in the study, two of whom (Subject 1 and 2) were examined at both 3 T and 7 T.

4.1.1 Example of DGE image

Post-processed DGE images for one healthy volunteer are shown in figure 4.1. The response to glucose differs between individuals, but all healthy subjects showed generally the same response steps, first seen as a slight DGE-signal increase in CSF (seen in ventricles) followed by an increase in vessels and then in tissue, as seen in the figure. In addition to the positive DGE-signal, negative signal can be seen in the ventricles after the initial positive signal.

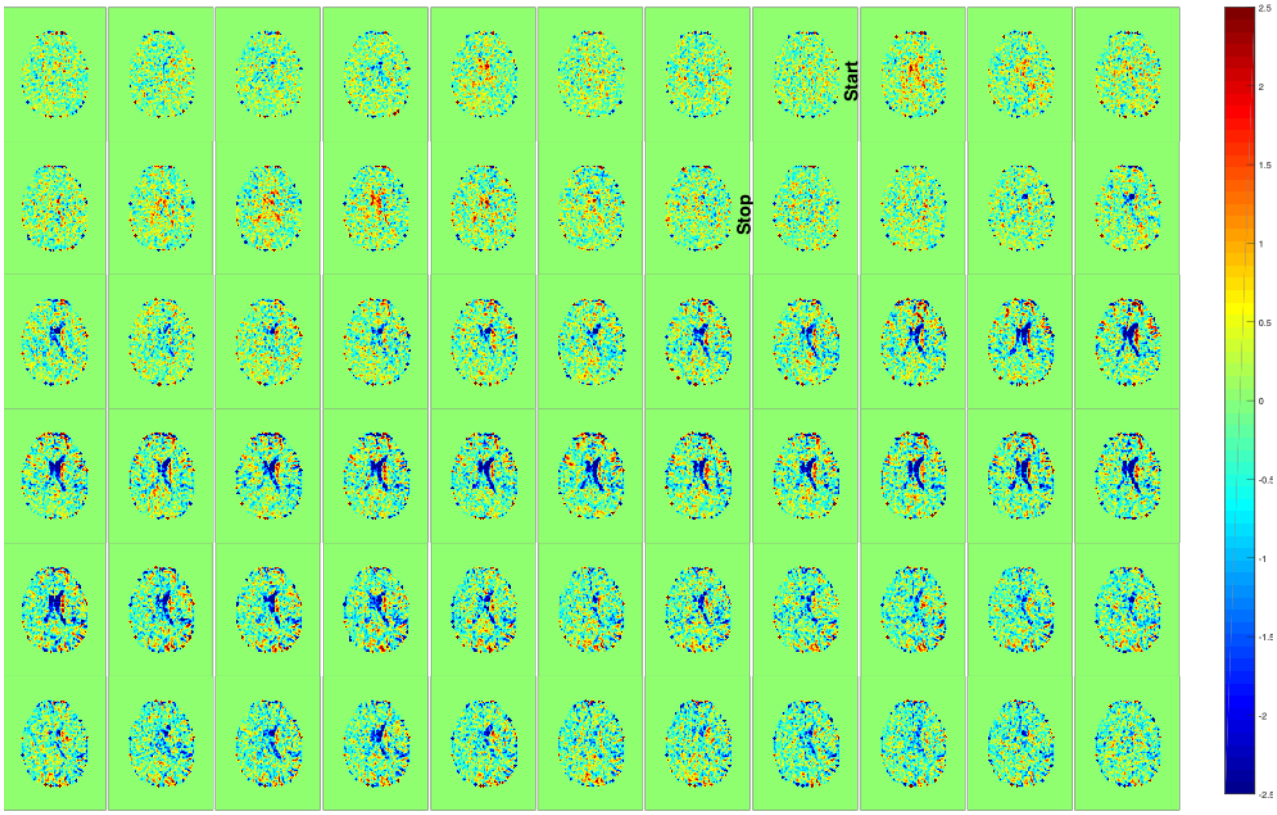

Figure 4.1 Example of DGE images from one healthy subject. Image 15 to 80 out of 123 are included in the figure, corresponding to approximately 9 minutes of imaging. The temporal resolution is 6.7 seconds and the total scan time is 15 minutes. The time interval between two consecutive images, read from left to right, is thus 6.7 seconds. START and STOP represents the start and finish of the glucose infusion, respectively. Positive DGE-signal is represented as red or yellow and negative DGE-signal is blue.

4.1.2 Dynamic response curves and blood glucose levels

Venous blood glucose levels as a function of time in four subjects measured during the 3 T experiment are shown in figure 4.2. The figure illustrates how the blood glucose levels in a peripheral vein differs between three of the subjects after administration of the same amount of glucose. Complete blood glucose curves were not achieved for two participants due to problems with the blood sampling. Those curves are not included in figure 4.2.

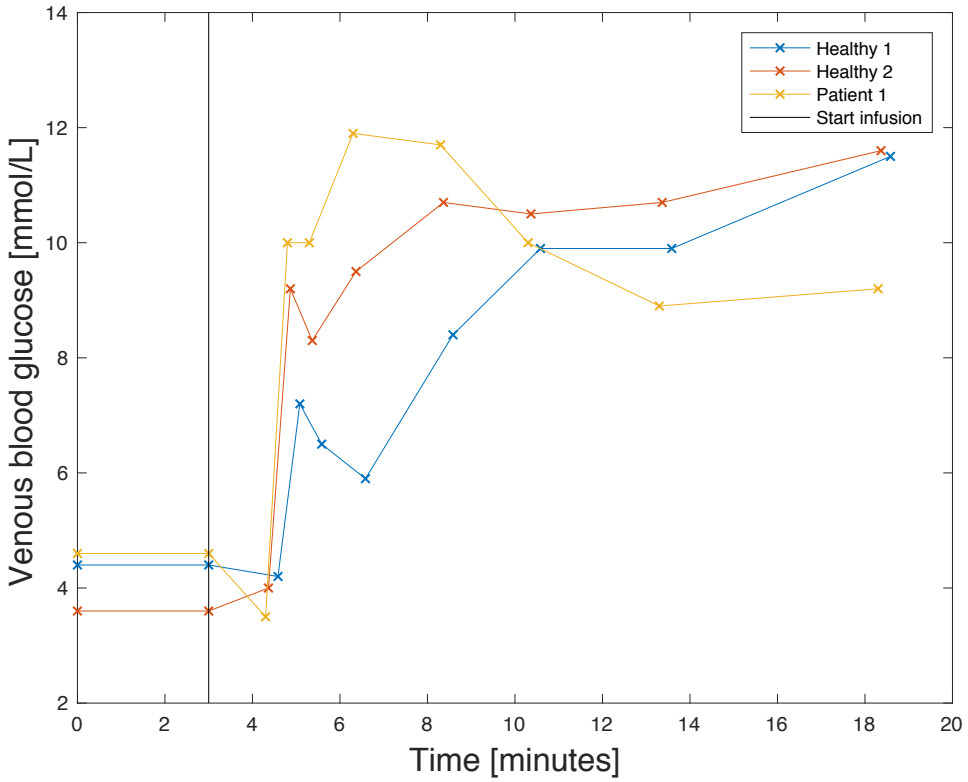

Figure 4.2 Venous blood glucose curves in 4 subjects. The intravenous glucose was administered after three minutes, indicated by the black vertical line.

Dynamic response curves from three healthy volunteers, examined at both 3 T and 7 T, are shown in figure 4.3. The black curves represent the signal change over time in an artery (ACA), which can be interpreted as the arterial input function (AIF). The green curves denote the response in white matter (WM), and the blue curve denote the venous blood glucose level as a function of time. The time is shifted so that the zero time point represents the starting time of glucose infusion (3 minutes into the dynamic sequence). The infusion duration for each subject is represented by a blue region. A signal increase approximately following the venous blood glucose curve can be seen in all subjects in the AIFs, while the tissue curve is rather constant.

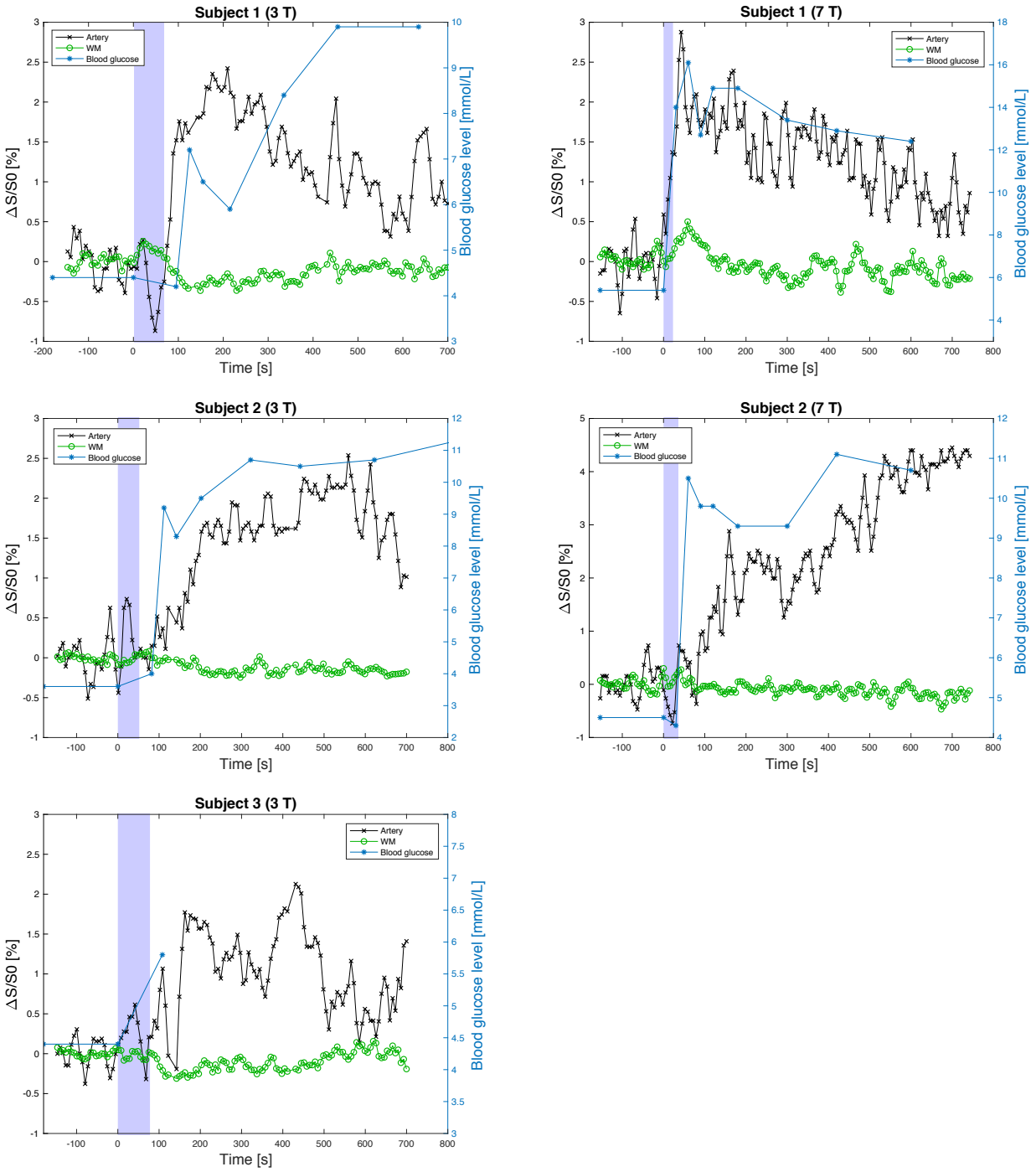

Figure 4.3 Dynamic response curves for three healthy volunteers. The normalized signal difference and the measured venous blood glucose levels are presented as a function of time. The blue area represents the infusion time duration. Curves acquired at 3 T are placed to the left for each subject. For participants examined at both 3 T and 7 T, the 7 T curves are placed to the right. Subject 3 lacks complete blood glucose curves, which is why only the initial part of the venous blood glucose curve is shown.

4.1.3 AUC images

Figure 4.4 shows 3 T DGE AUC images for 2-minute intervals from three healthy volunteers. The pre-infusion AUC images (AUC 0-2 minutes) are rather homogenous. An increase (red and yellow) in DGE-signal, presumably caused by the presence of glucose, can be seen initially in the ventricles in subject 1 and 3, immediately after the glucose infusion, followed by the vessels. A decrease (blue) is seen in the ventricles and other CSF-rich regions (e.g. sulci) after the initial increase. Alternating positive and negative values with the same shape next to each other might be caused by motion effects. Note that those are more prominent in the later AUC images, which are acquired at later times with respect to the baseline images.

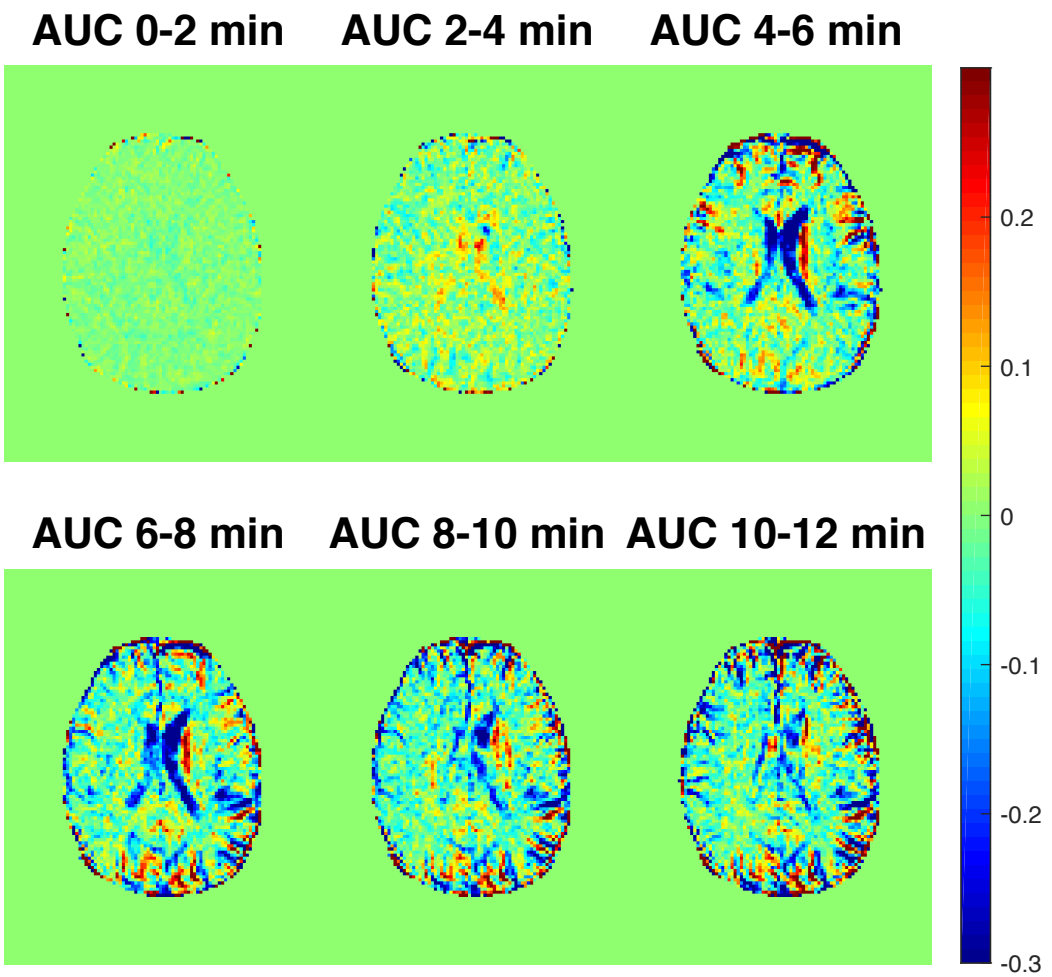

Figure 4.4a 3 T DGE AUC images for two-minute intervals in healthy volunteer number 1. A positive value (red and yellow) represents an increased glucose concentration in the voxel. The glucose infusion was started after three minutes.

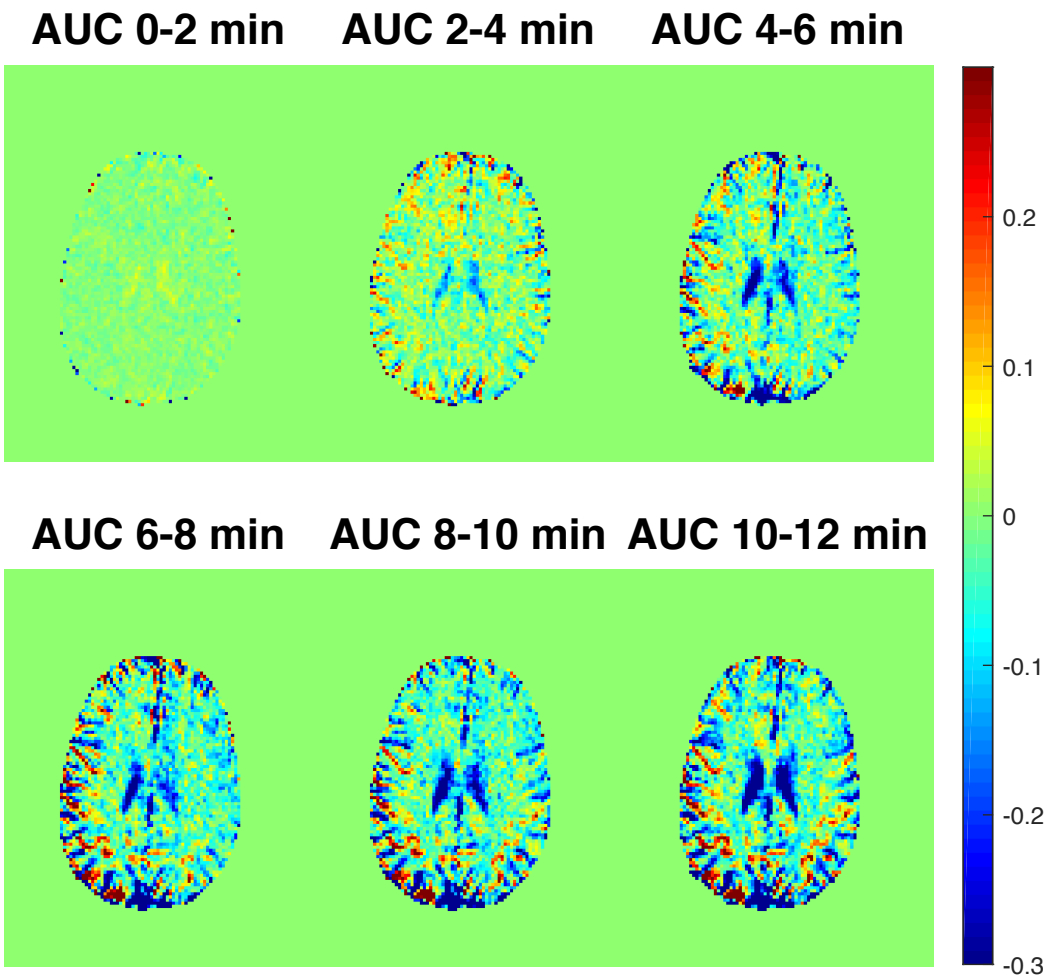

Figure 4.4b 3 T DGE AUC for healthy volunteer number 2.

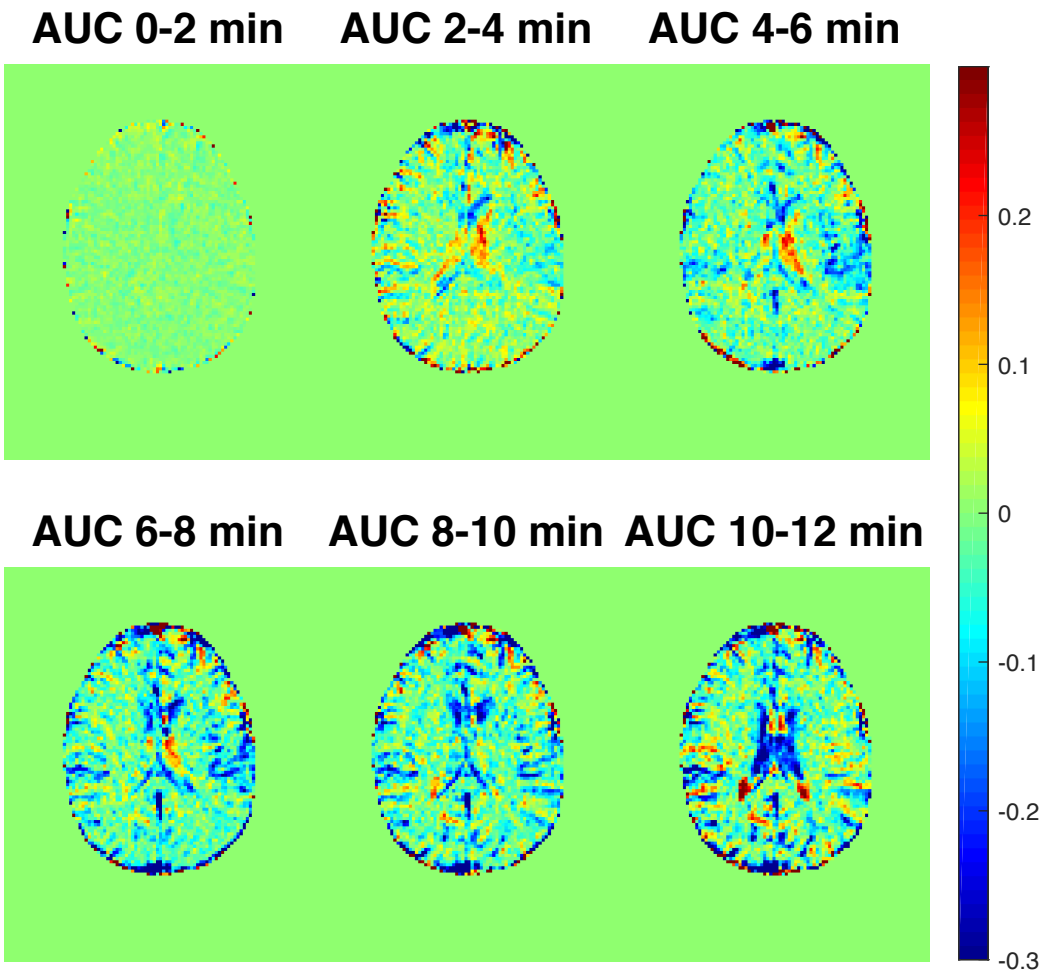

Figure 4.4c 3 T DGE AUC for healthy volunteer number 3.

DGE AUC images for two-minute intervals for healthy volunteer number 1 and 2 acquired at 7 T are presented in figure 4.5. Note that the range of the color scale is the same for all subjects at both 3 T and 7 T, and that the spatial resolution is different (2x2x6 mm^3 at 3 T compared to 3x3x6 mm^3 at 7 T). Larger differences (more red voxels) compared to the baseline image (0-2 minutes) can be seen in the 7 T images than in the 3 T images.

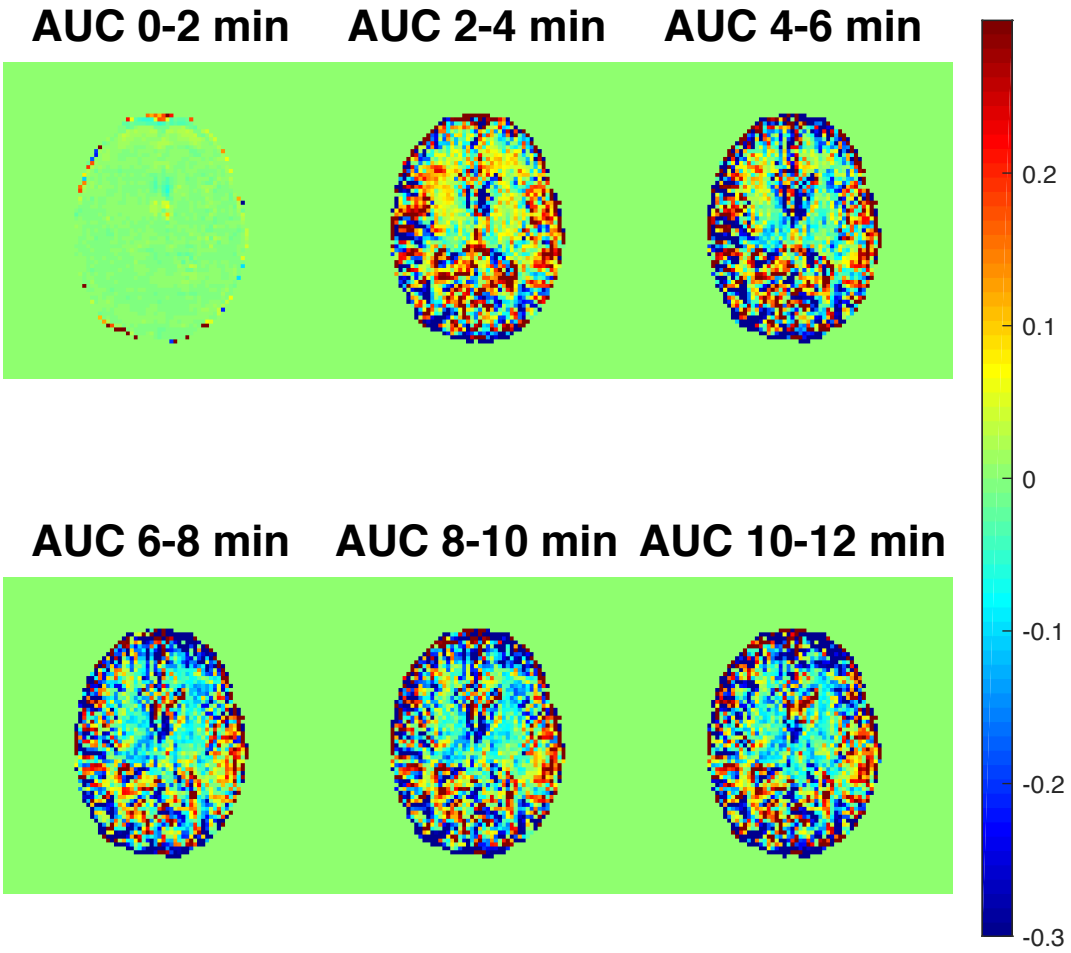

Figure 4.5a 7 T DGE AUC images for healthy volunteer number 1. A positive value (red and yellow) represents an increased glucose concentration in the voxel. The glucose infusion was started after three minutes.

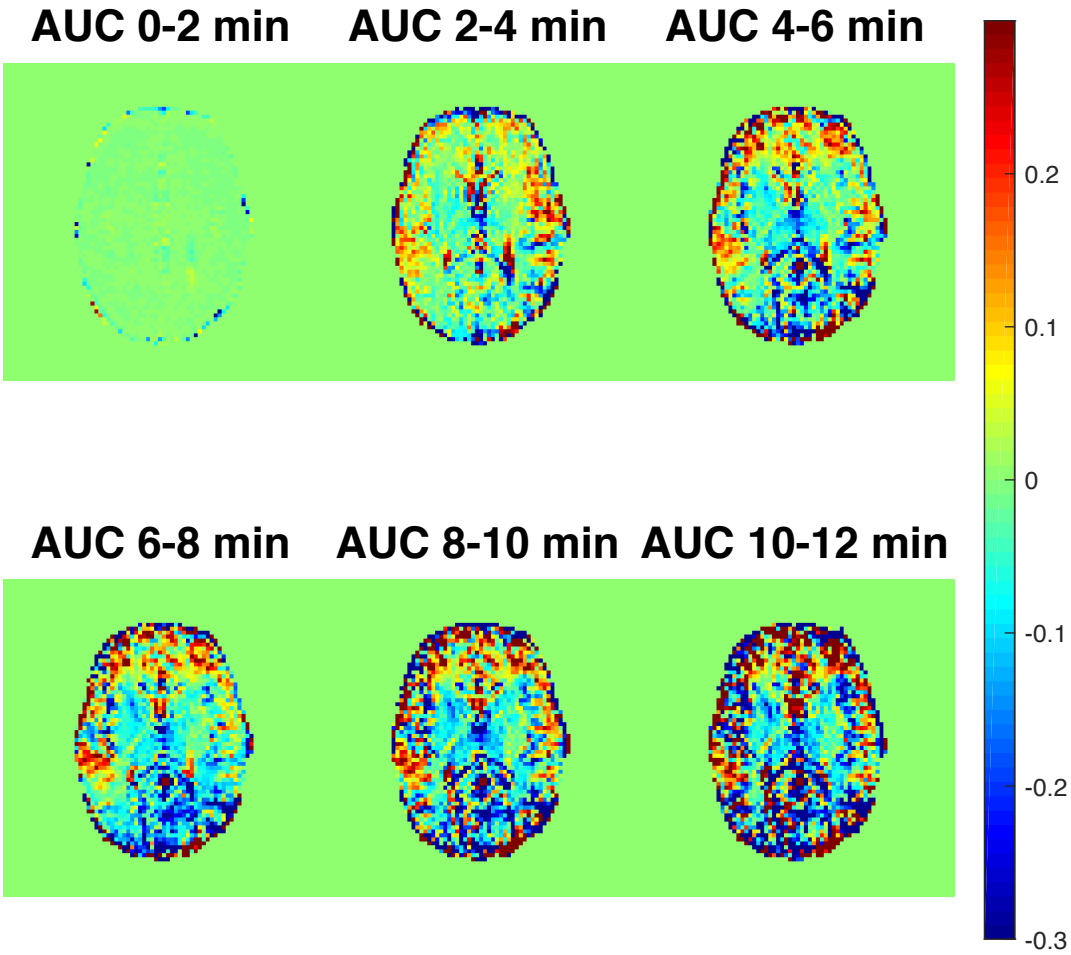

Figure 4.5b 7 T DGE AUC for healthy volunteer number 2.

To visualize the effects of motion, DGE AUC maps for two-minute intervals computed with and without retrospective motion correction are shown in figure 4.6.

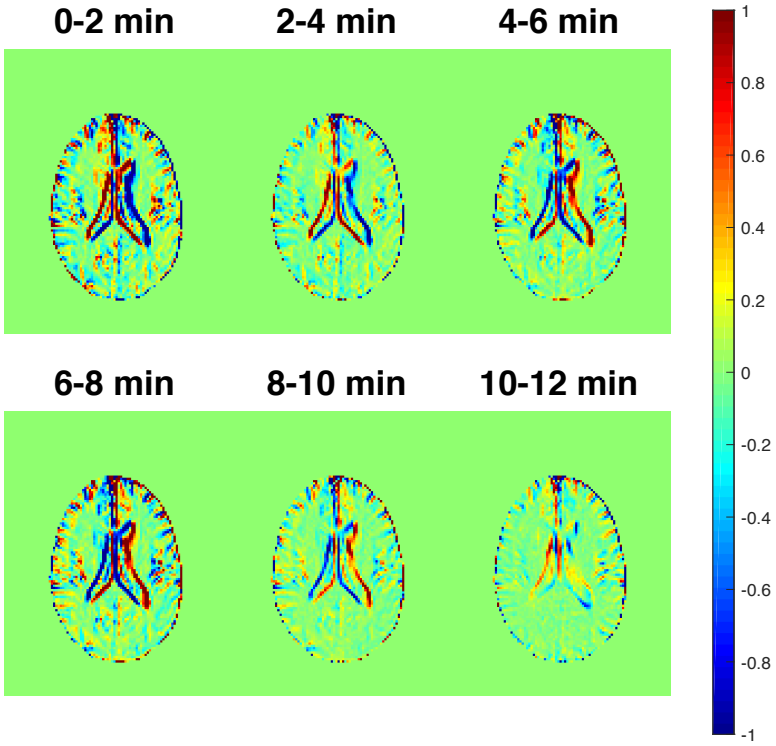

Figure 4.6a DGE AUC images of a fasting healthy volunteer without glucose infusion, calculated without motion correction.

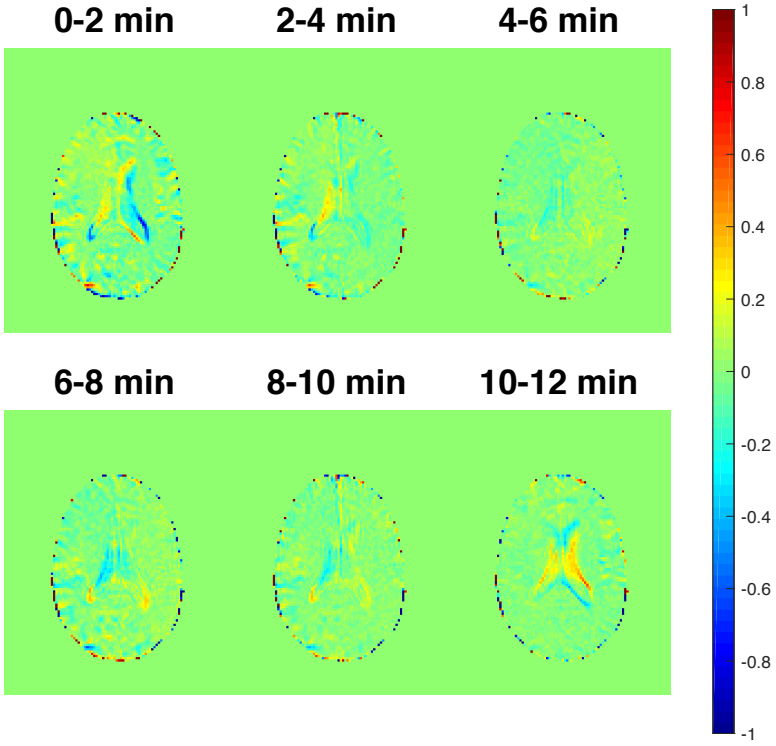

Figure 4.6b DGE AUC images of a fasting healthy volunteer without glucose infusion, calculated with motion correction.

4.2 Patients

2 patients with brain cancer participated in the study and were examined at 3 T. There is a difference in slice thickness between image types and a different slice orientation is used in the anatomical images.

Patient 1

A 52-year-old male that has previously undergone surgery for a brain tumor is shown in figure 4.7. The tumor is suspected to be a recurring tumor. Anatomical images, DCE AUC and DGE AUC images are shown in figure 4.7a. Enhancement of corresponding areas in the tumor region can be seen both in the DCE AUC image and in the DGE AUC images. Dynamic curves measured in regions of interest in the glucose-enhanced images are shown in figure 4.7b. The tissue in the tumor area has a late response compared to the venous blood glucose level.

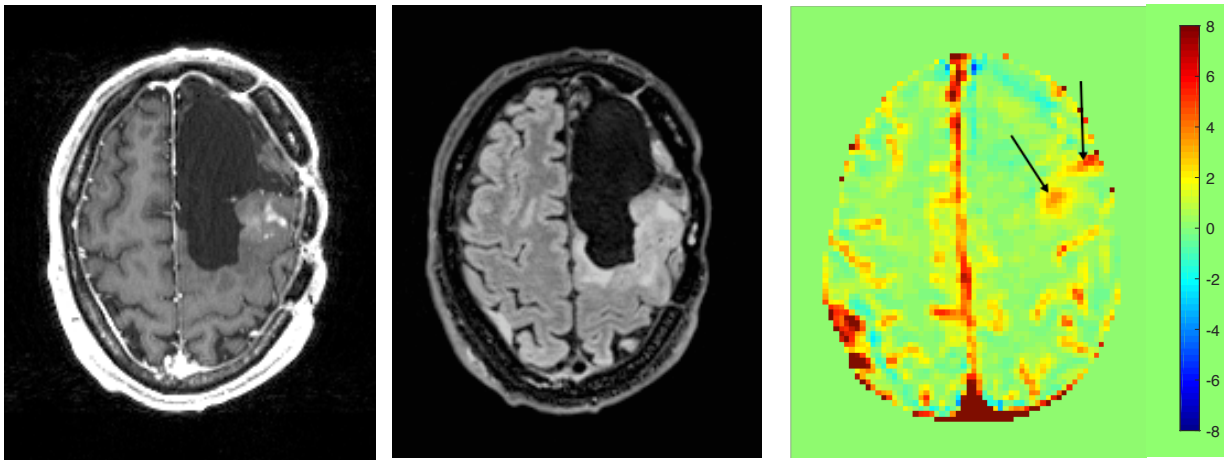

GdT1w (MPRAGE)
1x1x1 mm³

T2w (FLAIR)
1x1x1 mm³

DCE AUC
2x2x4 mm³

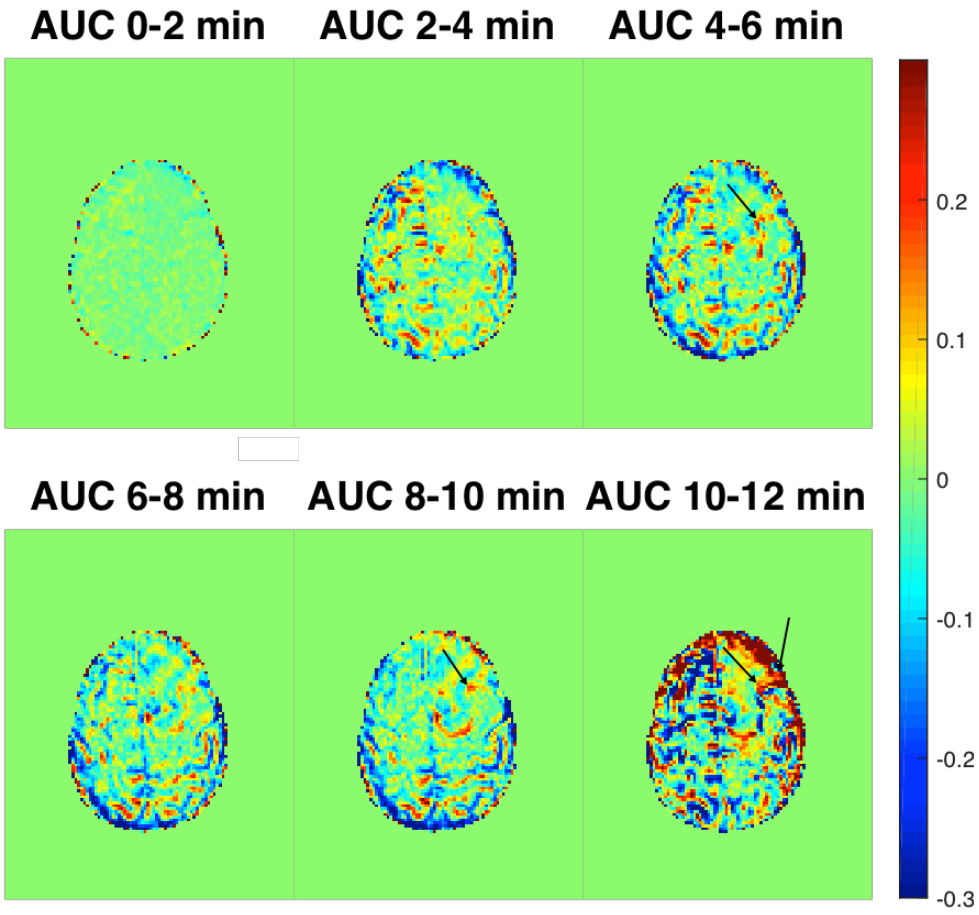

DGE AUC (2x2x6 mm³)

Figure 4.7a Anatomical images, DCE AUC for a post-infusion time interval and DGE AUC for two-minute intervals of a patient with brain tumor. The arrows represent regions in the tumor area that are enhanced both in the DCE AUC and DGE AUC images.

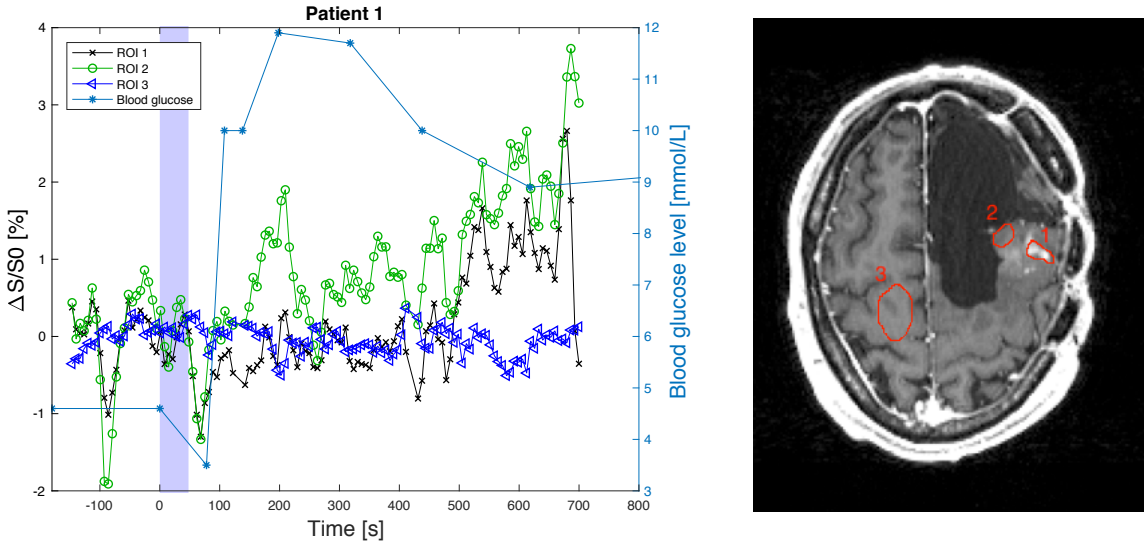

Figure 4.7b DGE time curves (left) in different brain regions, marked in the image to the right. ROI 1 represents the gadolinium-enhancing tumor region, ROI 2 represents an area adjacent to the tumor and ROI 3 is placed in contralateral white matter.

Patient 2

The other patient was a 76-year-old male with a solitary brain tumor. Anatomical images, DCE AUC and DGE AUC images are shown in figure 4.8a. The tumor is remarkably enhanced in the DCE AUC image, but not distinguishable in the DGE AUC images. Dynamic curves measured in regions of interest in the glucose-enhanced images are shown in figure 4.8b.

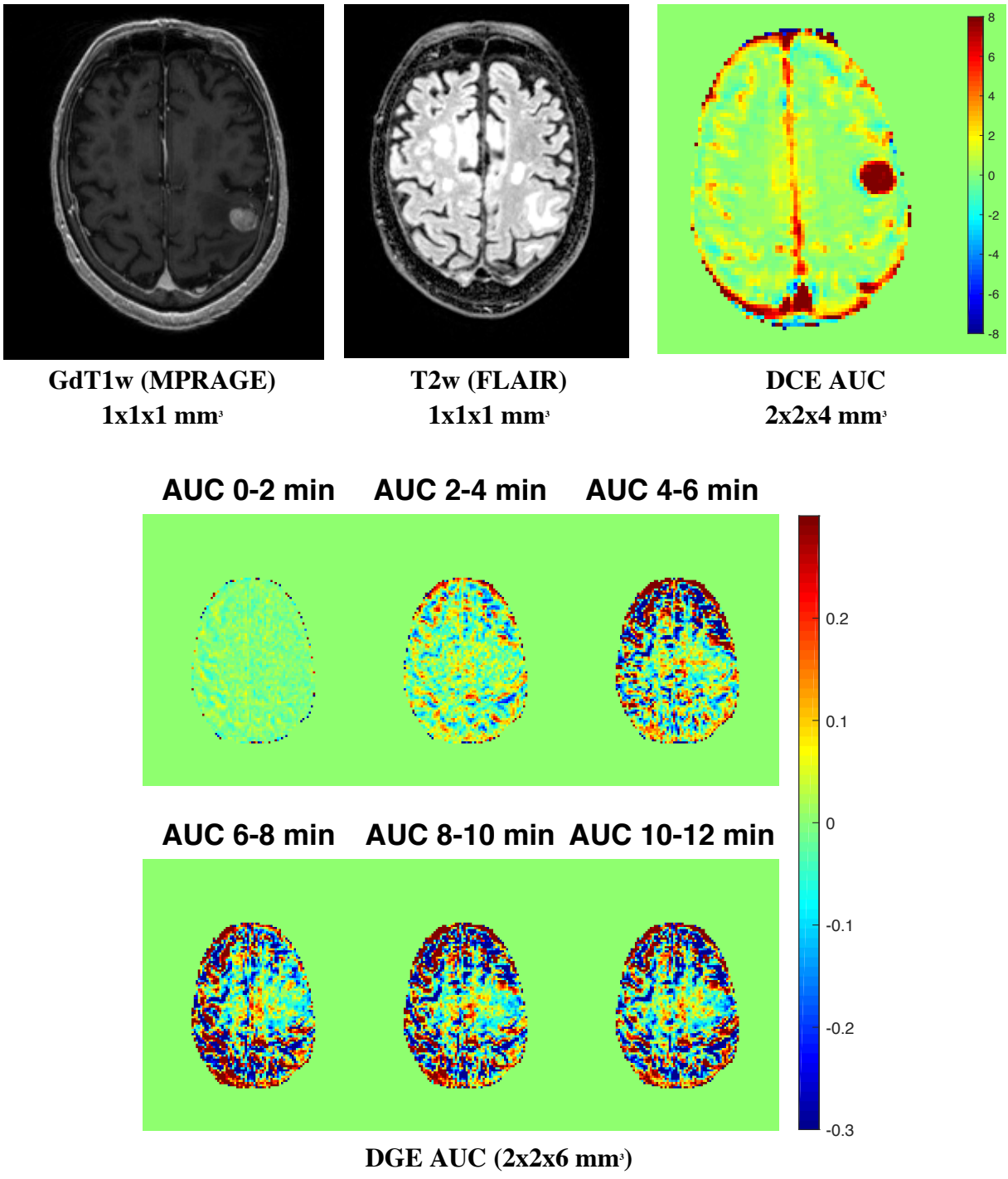

Figure 4.8a. Anatomical images, DCE AUC for a post-infusion time interval and DGE AUC for two-minute intervals of a patient with brain tumor. The anatomical images are acquired with a different slice position than the DGE and AUC images.

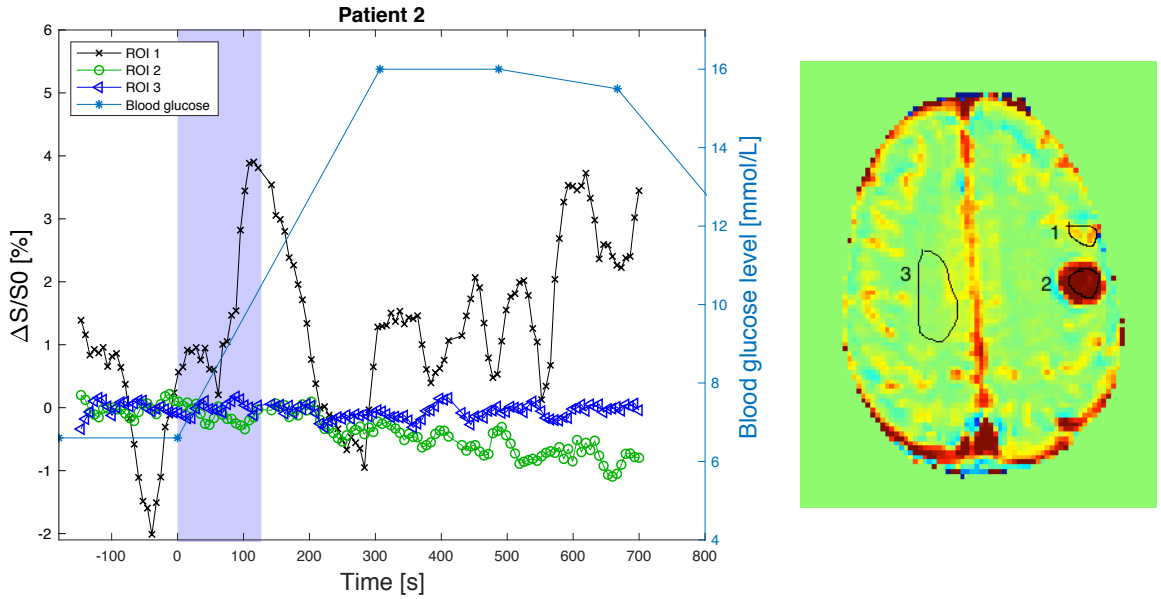

Figure 4.8b DGE time curves (left) in different brain regions, marked in the AUC DCE-image to the right. ROI 1 represents an area close to the tumor, ROI 2 is placed the tumor core and ROI 3 is placed in contralateral white matter. Due to problems with the blood sampling, there are no information about the venous blood glucose level between 0 and 300 seconds.

5 Discussion

This study indicates that glucoCEST is applicable at 3 T. What can be concluded so far is that it is possible to get DGE contrast at 3 T. The interpretation of the images is not straightforward, and more information is needed to determine what physiological and/or pathological processes are shown in the images. For this, a glucose tracer kinetic model is needed, but that is out of the scope of this project, albeit a topic for future research. The experimental results were evaluated qualitatively, partly due to the low number of participants.

5.1 Dynamic response curves, blood glucose curves and DGE images

All healthy subjects show an individual glucose response, which can be seen as a difference in shape and magnitude in the AIFs, as well as in figure 4.2 (the plot representing the venous blood glucose level as a function of time for four participants). The main reason for these differences can be addressed to the individual insulin response. After the glucose infusion, the blood glucose level rises to a hyperglycemic level, which will trigger the pancreas to excrete insulin. The insulin will increase glucose uptake in peripheral tissues (e.g. muscles) by activating the insulin-dependent glucose transporters. This process will lower the blood glucose level, implicating that a rapid or large insulin response will result in a quick drop in blood glucose level after the rise caused by the glucose infusion. A slow or modest insulin-response will lead to a slower glucose metabolism which will manifest as a slowly decaying curve. The individual insulin response will therefore affect the AIFs, because the blood glucose level is affected. Insulin is not believed to increase glucose transport to the brain, this transport is instead relying on the concentration gradient between the blood and the brain (37). Under steady-state conditions, the glucose concentration in brain tissue is around 20% of that in arterial blood (37), so only a small fraction of the glucose will be transported over the BBB. However, the AIF and the venous blood glucose curve are generally similar in shape, suggesting that the blood glucose curves can serve as a guideline to how each individual reacts to the glucose infusion, and therefore support the evaluation of the DGE-signal. Long plastic tubes were used for blood sampling, and in some individuals, it was challenging to take blood samples, resulting in incomplete blood glucose curves. In all the AIFs in figure 4.3, the arterial signals show larger fluctuations than the WM signals, probably due to pulsations in the vessels.

The glucose is administered into the blood and is transported from the capillaries over the BBB mainly by GLUT1 transporter proteins, entering the extravascular extracellular space (EES). Subsequently, the glucose is transported into the cells, where it is metabolized. This process leads to a disappearance of the glucoCEST signal. The glucoCEST signal will therefore originate mainly from vessels and EES (1, 40). The exchangeable protons remain

during the first steps of glycolysis, but the intracellular contribution is probably small compared to the signal from the other compartments.

In dynamic perfusion imaging with gadolinium, AIFs are used to calculate perfusion and perfusion related parameters (e.g. blood flow, blood volume and tissue permeability). These parameters can be extracted either by deconvolution of the AIF and the tracer concentration curve, or by application of a compartment model (41). The assumptions made in kinetic models for gadolinium tracers does not hold when glucose is used as contrast agent, since the physiological processes and therefore the distribution of the contrast agent is different. The main difference between gadolinium and glucose is that gadolinium circulates in the blood and does not enter cells or penetrate the BBB (unless it is damaged), while glucose crosses the BBB and enters the cells, where it is rapidly metabolized. Another important disparity between gadolinium and glucose is that glucose is present in the system before the infusion, meaning that the baseline level is non-zero. It is therefore important that the subjects are fasting, so that the change in glucose concentration can be measured relative to a stable baseline level.

Similar models exist for FDG-PET imaging, where glucose metabolism can be measured from radioactive glucose (fluorodeoxyglucose (^{18}F-FDG)). This approach is not applicable to glucoCEST, since the PET-tracer enters the cell where it accumulates instead of being metabolized. For these reasons, it is still unclear which parameters that can be calculated from DGE experiments in practice.

The magnitude of the AIFs is affected by partial volume effects (PVE) with surrounding tissue. Due to the relatively large voxel size (thick slice, large pixels), the chosen voxel will not contain merely blood. Tissue and CSF might be included, which will lower the averaged DGE-signal. The impact of PVEs will be reduced with a better spatial resolution.

The DGE-signal is affected by motion, for example head movements, pulsations and volumetric changes of ventricles and vessels. Since the images are based on small differences, even small movements will affect the resulting DGE and DGE AUC images by creating false signal differences. Motion effects are more prominent in AUC images since it is a stack of DGE images, so that differences due to motion will accumulate and possibly obfuscate the differences caused by saturation transfer. This is visualized in figure 4.6, where DGE AUC images of a fasting healthy volunteer were calculated with and without performing retrospective motion correction. The healthy volunteer can be assumed to have a stable blood glucose level and was lying as still as possible. The DGE-signal differences seen in figure 4.6a can therefore be argued to arise primarily from internal motion such as pulsations and related volumetric ventricular changes. Motion is an issue due to the small signal changes that are detected in glucoCEST, and to the relatively long scan time.

In the arterial dynamic curves, a signal change (approximately 2-4% compared to baseline) corresponding to an increase in glucose concentration, can be seen rapidly after the glucose infusion. The DGE and DGE AUC images show negative signal mainly in the ventricles, but also in other regions where CSF is present.

An explanation to this hypointensity can be found by considering the Z-spectra in different types of brain tissue. At baseline glucose levels, the Z-spectrum in CSF is narrower than in tissue. When the glucose concentration in CSF increases, the Z-spectrum (the line shape of direct water saturation) will broaden, which will manifest as a positive signal (as seen in the ventricles for subject 1 and 3 in the early DGE AUC images (2-4 minutes) in figure 4.4). Subsequently, the volume of the ventricles will increase as a physiological response to the increased glucose concentration (42), causing the Z-spectrum to narrow again. The negative (blue) signal in DGE images is thus due to an apparent glucose concentration decrease, caused by the relative glucose concentration decrease because of the volumetric changes of the ventricles. This reasoning can be verified by comparing a Z-spectra calculated from a ROI in CSF (ventricle), normal brain tissue (white matter) and vessels, collected before and after glucose infusion in a healthy volunteer, shown in figure 5.1.

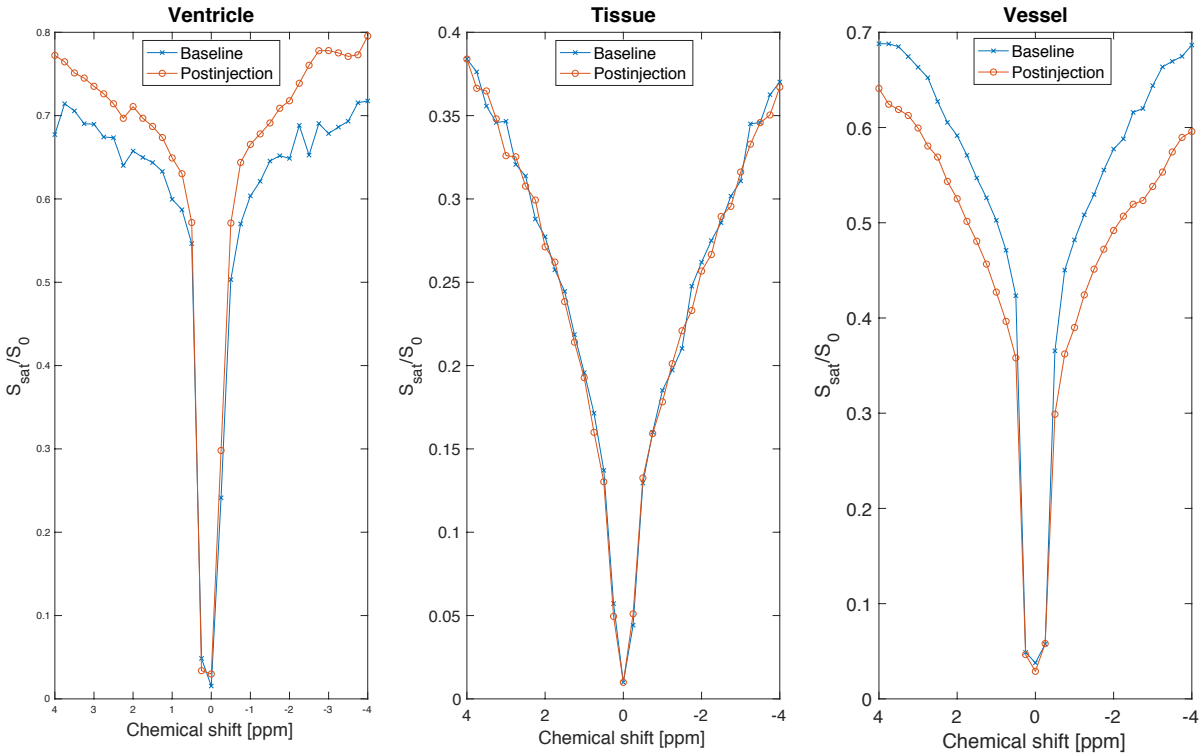

Figure 5.1 Z-spectra calculated from ROIs in a ventricle, in tissue (white matter) and in a vessel. The Z-spectrum in CSF (ventricle) is narrower than in tissue and vessels. After glucose infusion, a slight narrowing of the Z-spectrum can be seen. The spectrum in tissue does not change, but the Z-spectrum calculated from a ROI placed in a region rich in vessels is broadened after glucose infusion, due to the increased glucose concentration in blood.

The DGE-signal (equation 3.1) represents the signal change relative to the baseline. From the Z-spectra in figure 5.1 above, it becomes clear that CSF-rich regions will be characterized by a negative DGE-signal since the signal in a voxel, measured after saturation at 2 ppm, is larger after glucose infusion than at baseline. The post-injection Z-spectra are collected after the dynamic scan (>12 minutes after the glucose infusion), so these differences can be expected to be more noticeable directly after the glucose infusion (e.g. in the dynamic images). This provides an explanation to the negative (blue) signal seen in DGE AUC images. The presence of CSF will also affect the DGE-signal magnitude through PVEs, because when both CSF and blood is present in a voxel, the measured signal will include contributions from the narrower Z-spectrum in CSF. This will lower the observed DGE-signal, and will affect the measured AIFs, as discussed earlier. The Z-spectrum in tissue is broader and lower than the others (note the difference in the y-axis), and this is probably due to the presence of macromolecules, which increases the contribution from other saturation transfer effects such as MTC and NOE. The shape of the tissue-spectrum does not seem to depend on glucose concentration, since it does not change after the glucose infusion. From this, the conclusion that the contribution from other MT effects is constant over the experiment can be drawn.

One simple solution to this problem is to show only the positive DGE-values, as shown in figure 5.2. The drawback of this visualization is that the false positive signals caused by motion are more difficult to identify. A better solution for future studies would therefore be to remove CSF signals using suppression techniques.

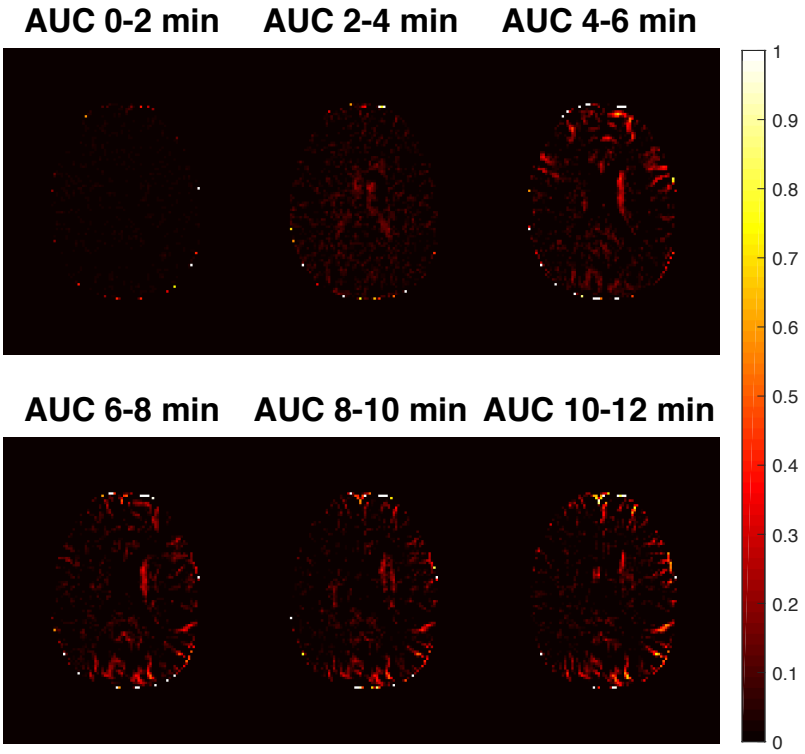

Figure 5.2 DGE AUC images from subject 1 at 3 T. Only positive values are included.

5.2 Comparison of glucoCEST at 7 T and 3 T.

In general, and as expected, a somewhat higher CEST-effect can be seen in the 7 T results compared to the results at 3 T. The higher CEST-effect can be seen as slightly higher amplitude in AIFs at 7 T and can also be observed in the DGE AUC images (figure 4.4 compared to 4.5) as a higher intensity (more red voxels) in the 7 T images. This can be a reason to why it seemed easier to find AIFs in 7 T images than in 3 T images.

Moreover, the higher CEST-effect at 7 T can be seen in the dynamic response curves (figure 4.3) in tissue. For instance, no effect is noticeable in the response curves in WM when the glucose arrives in 3 T images, but at 7 T, a small increase (around 0.5 % when images are normalized to S_0) that follows the AIF peak can be seen, as indicated in figure 5.3. The absence of signal increase in 3 T tissue curves is probably due to lower SNR in combination with a lower CEST-effect and it is an example of the current limitations for glucoCEST at 3 T.

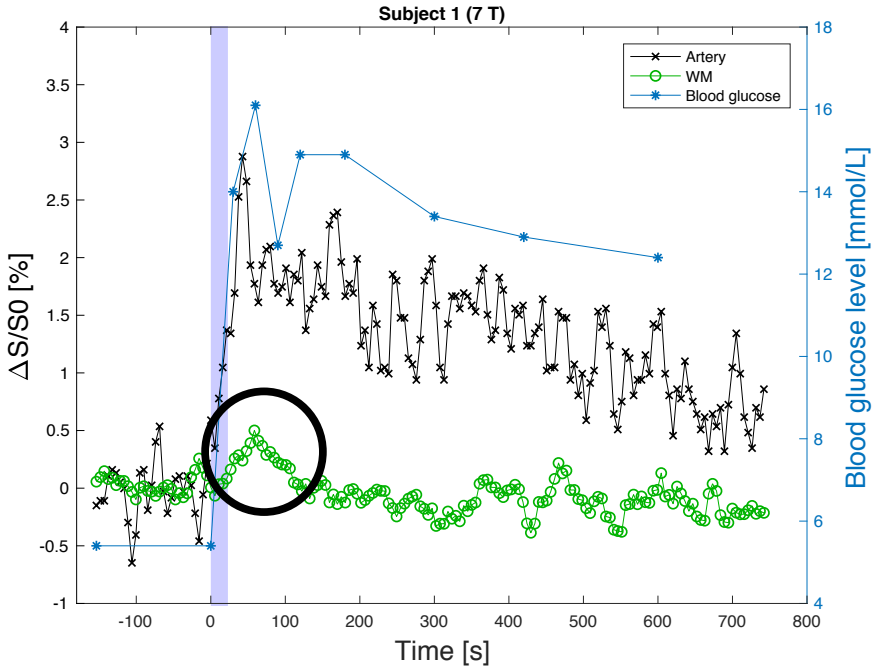

Figure 5.3 Dynamic response curve in healthy volunteer number 1. The circle emphasizes a response in WM that may reflect the AIF shape, but this small peak is hardly distinguishable from the noise level overall.

The same color scale is used for all DGE AUC images and the maximum and minimum values are compromised to be suitable for visualization of both 3 T and 7 T results using the same range. Therefore, the range of the color scale may not be optimal for each individual AUC map. The 7 T DGE AUC images in figure 4.5 would for example benefit from an extended color scale range because the DGE-signal differences are larger overall at 7 T than at 3 T. It should be noticed that the in-plane resolution differs between 7 T (3x3 mm^2) and 3 T (2x2 mm^2), which might be deceptive when AUC images are compared. The larger voxel size used at 7 T also suggests that PVEs have more impact on the 7 T results.

The differences between glucoCEST at 3 T and 7 T can be further investigated via equation 2.2. For example, the longer T_1 at 7 T will allow the saturation to remain longer, leading to a larger PTR and thus a higher glucoCEST-signal. This is one reason for the higher CEST-effect seen in 7 T DGE images and dynamic response curves. Another benefit of 7 T protocol is the longer saturation duration (50 ms · 32 pulses = 1.6 s at 7 T compared to 99.8 ms · 5 pulses = 0.5 s at 3 T), which increases the CEST-effect.

A higher RF amplitude (B_1) will give more DS and more MTC effects. MTC is present over all frequencies but can be assumed to be the same for all images (if B_1 is stable) and will thus be negligible when the signal difference is studied, as in DGE images. The DGE approach does also make the result less susceptible to magnetic field inhomogeneities,

since those can be assumed to be similar in each dynamic image. However, the same B_1 (2 μT) was used at both field strengths. The same amount of glucose (50 mL) was infused at both 7 T and 3 T, so the glucose concentration can be assumed to be similar, even though there might be a difference in body size and blood volume between the participants.

The chemical shift, $\Delta\omega_{sw}$, increases with field strength, which is why DS of water will be more prominent at 3 T than at 7 T since the glucose resonance frequency is closer to the water resonance frequency at lower field strength. This will decrease the sensitivity of glucoCEST at 3 T, since the glucose differences will be more difficult to distinguish.

At first, it might seem counterintuitive that a smaller saturation frequency was used at 7 T (1.2 ppm) than at 3 T (2.0 ppm) since the chemical shift increases with increased magnetic field strength. The water protons in the glucose hydroxyl group will get slightly different resonance frequencies when placed in a magnetic field, and this frequency separation is larger at 7 T. The chemical shift depends on field strength, temperature (26) and on the duration of the applied RF saturation pulse. Three of the hydroxyl protons have resonance frequencies around 1.2 ppm and the two others are resonating at roughly 2 and 3 ppm respectively (4, 26). At this 7 T-experiment, the approach is to target the three 1.2 ppm protons. At 3 T, the separation between the different resonance frequencies decreases so that each individual peak will be less distinguishable. Hence, it is more beneficial to target the whole averaged OH-resonance peak. The RF offset frequency of choice will therefore depend on field strength and the properties of the RF-pulse.

Overall, a higher CEST-effect was seen in 7 T images, but the 3 T results follow the same pattern. It was easier to find AIFs in 7 T images, even though the spatial resolution was worse, meaning more PVEs. This can be interpreted as higher specificity at 7 T. However, both 3 T and 7 T DGE images showed an increase in vessels and it was possible to find AIFs in all subjects. This allows us to draw the conclusion that DGE imaging is feasible at 3 T.

5.3 Tumor enhancement

For patients, DCE-imaging was also included in the protocol. The DCE technique employs the T1-shortening caused by gadolinium. A bolus of contrast agent is administered during rapid T1-weighted imaging and the signal increases where the gadolinium concentration is high. Pharmacokinetic modelling is normally used to extract perfusion parameters from the DCE-data. In this case, the DCE-data is instead used to calculate an AUC-map showing the signal change after contrast agent administration (equation 3.3). Gadolinium and glucose have different kinetics, as previously discussed, but the DCE-AUC image can be compared to the DGE-images because it indicates regions of increased vascularity and BBB-disruption.

In patient 1, the tumor-area is distinguishable from the normal tissue and comparable to the DCE AUC in the same region. In addition, the DGE AUC image shows features that are not seen in the DCE AUC image, for example the region inside the circle in figure 5.4 below. The physiological background of these effects is not entirely clear. One interpretation might be that the marked region has a slightly altered BBB-permeability or increased number of glucose transporters, that allows more glucose to enter the EES. It could also simply be vessels providing the tumor with blood.

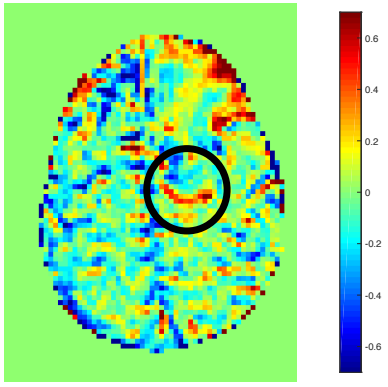

Figure 5.4. DGE AUC for a 4-minute post-infusion time interval.

In the dynamic curves, figure 4.7b, the signal change is measured in three different ROIs. The first one (ROI 1) corresponds to the region that showed contrast enhancement in the T_1-weighted post-gadolinium image. This region shows a late response (peaks after 500 seconds), indicating that it represents tumor tissue rather than blood vessels. ROI 2 was placed in a region that showed a signal change in both DGE AUC and DCE AUC images. This area does show a late DGE-signal increase but is less stable and a peak is seen after the glucose infusion, insinuating that it corresponds to a vascular region. ROI 3, placed in contralateral WM, show a constant signal similar to the signal in WM in healthy subjects.

The results from patient 2 (figure 4.8) are more difficult to interpret. An infusion time twice as long as in the other subjects was used, and the patient was moving during the scan. Additionally, the venous blood glucose curve is incomplete due to difficulties with the blood sampling. The tumor region is rather homogeneous, and in later DGE AUC images, a slight decrease (negative signal) can be seen. This can also be seen in the dynamic curve from the ROI placed in the tumor core. One reason for the negative signal in the tumor might be that the tumor has high metabolic activity and that the EES will be cleared from glucose. If the tumor is poorly perfused, no increase in DGE-signal will then be seen. While not clear at this instance, this may provide valuable information that can be used for tumor grading and differentiation in the future. The signal in ROI 1 is showing large intensity variations, which may be because the region is close to the boundaries of the brain,

where motion effects are more prominent. The fluctuations and the shape of the signal curve might also suggest that this region includes a large amount of vessels.

In summary, more patients need to be examined to draw any firm conclusions regarding tumor enhancement. Changes in the DGE-signal can be seen in the regions with lesions after glucose infusion, and enhancement of the tumor region comparable to the DCE AUC image can be seen in DGE AUC images of patient 1, indicating that DGE imaging of brain cancer is possible at 3 T.

6 Conclusion

In this master thesis project, glucoCEST has been used to acquire glucose-enhanced images of both healthy volunteers and brain tumor patients at 3 T. Although the number of participants was small (n = 5) it is possible to draw the conclusion that glucoCEST is feasible at 3 T. The arguments for this is that a change in the water signal was seen in all subjects after the blood glucose level had been raised using an intravenous injection of D-glucose. Additionally, tumor enhancement was obtained in one patient. In the comparison of 3 T and 7 T images, it was concluded that the experiment on 7 T yielded a somewhat higher CEST-effect suggesting higher specificity.

This work provides a first step towards clinical use of natural sugar as a biodegradable contrast agent. The future improvements of the approach include, but are not limited to, higher coverage, longer saturation time, CSF suppression and the implementation of a kinetic model to enable assessment of perfusion information. GlucoCEST seems to hold the possibility of becoming an alternative or complement to FDG-PET and Gd-enhanced MRI in the future.

7 References

1. Chan KW, McMahon MT, Kato Y, Liu G, Bulte JW, Bhujwalla ZM, et al. Natural D-glucose as a biodegradable MRI contrast agent for detecting cancer. Magnetic Resonance in Medicine. 2012;68(6):1764-73.

2. Xu X, Chan KW, Knutsson L, Artemov D, Xu J, Liu G, et al. Dynamic glucose enhanced (DGE) MRI for combined imaging of blood-brain barrier break down and increased blood volume in brain cancer. Magnetic Resonance in Medicine. 2015;74(6):1556-63.

3. Xu X, Yadav NN, Knutsson L, Hua J, Kalyani R, Hall E, et al. Dynamic Glucose-Enhanced (DGE) MRI: Translation to Human Scanning and First Results in Glioma Patients. Tomography. 2015;1(2):105-14.

4. Walker-Samuel S, Ramasawmy R, Torrealdea F, Rega M, Rajkumar V, Johnson SP, et al. In vivo imaging of glucose uptake and metabolism in tumors. Nature Medicine. 2013;19(8):1067-72.

5. Socialstyrelsen, Cancerfonden. Cancer i siffror 2013. 2013-6-5.

6. Errante Y, Cirimele V, Mallio CA, Di Lazzaro V, Zobel BB, Quattrocchi CC. Progressive increase of T1 signal intensity of the dentate nucleus on unenhanced magnetic resonance images is associated with cumulative doses of intravenously administered gadodiamide in patients with normal renal function, suggesting dechelation. Investigative Radiology. 2014;49(10):685-90.

7. Kanda T, Ishii K, Kawaguchi H, Kitajima K, Takenaka D. High signal intensity in the dentate nucleus and globus pallidus on unenhanced T1-weighted MR images: relationship with increasing cumulative dose of a gadolinium-based contrast material. Radiology. 2014;270(3):834-41.

8. Robert P, Lehericy S, Grand S, Violas X, Fretellier N, Idee JM, et al. T1-Weighted Hypersignal in the Deep Cerebellar Nuclei After Repeated Administrations of Gadolinium-Based Contrast Agents in Healthy Rats: Difference Between Linear and Macrocyclic Agents. Investigative Radiology. 2015;50(8):473-80.

9. McDonald RJ, McDonald JS, Kallmes DF, Jentoft ME, Murray DL, Thielen KR, et al. Intracranial Gadolinium Deposition after Contrast-enhanced MR Imaging. Radiology. 2015;275(3):772-82.

10. Scott JN, Brasher PM, Sevick RJ, Rewcastle NB, Forsyth PA. How often are nonenhancing supratentorial gliomas malignant? A population study. Neurology. 2002;59(6):947-9.

11. van Zijl PC, Jones CK, Ren J, Malloy CR, Sherry AD. MRI detection of glycogen in vivo by using chemical exchange saturation transfer imaging (glycoCEST). Proceedings of the National Academy of Sciences. 2007;104(11):4359-64.

12. Grobner T. Gadolinium - a specific trigger for the development of nephrogenic fibrosing dermopathy and nephrogenic systemic fibrosis? Nephrology Dialysis Transplantation. 2006;21(4):1104-8.

13. Morcos SK. Extracellular gadolinium contrast agents: differences in stability. European Journal Of Radiology 2008;66(2):175-9.

14. Rogosnitzky M, Branch S. Gadolinium-based contrast agent toxicity: a review of known and proposed mechanisms. Biometals. 2016;29(3):365-76.

15. Kanda T, Osawa M, Oba H, Toyoda K, Kotoku J, Furui S. High Signal Intensity in Dentate Nucleus on Unenhanced T1-weighted MR Images: Association with Linear versus Macrocyclic Gadolinium Chelate Administration. Radiology. 2015;275(3):803-9.

16. Radbruch A, Weberling LD, Kieslich PJ, Eidel O, Burth S, Kickingereder P, et al. Gadolinium retention in the dentate nucleus and globus pallidus is dependent on the class of contrast agent. Radiology. 2015;275(3):783-91.

17. Marckmann P, Skov L, Rossen K, Dupont A, Damholt MB, Heaf JG, et al. Nephrogenic systemic fibrosis: suspected causative role of gadodiamide used for contrast-enhanced magnetic resonance imaging. Journal of the American Society of Nephrology. 2006;17(9):2359-62.

18. Quattrocchi CC, Mallio CA, Errante Y, Cirimele V, Carideo L, Ax A, et al. Gadodiamide and Dentate Nucleus T1 Hyperintensity in Patients With Meningioma Evaluated by Multiple Follow-Up Contrast-Enhanced Magnetic Resonance Examinations With No Systemic Interval Therapy. Investigative Radiology. 2015;50(7):470-2.

19. EMA/625317/2017. EMA's final opinion confirms restrictions on use of linear gadolinium agents in body scans. 23/11/2017

20. FDA warns that gadolinium-based contrast agents (GBCAs) are retained in the body; requires new class warnings. Safety Announcement 12-19-2017.

21. Gulani V, Calamante F, Shellock F, Kanal E, Reeder S. Gadolinium Deposition in the Brain: Summary of Evidence and Recommendations. The Lancet Neurology.16(7):564-70.

22. van Zijl PCM, Yadav NN. Chemical exchange saturation transfer (CEST): What is in a name and what isn't? Magnetic Resonance in Medicine. 2011;65:927-48.

23. Ward KM, Aletras AH, Balaban RS. A new class of contrast agents for MRI based on proton chemical exchange dependent saturation transfer (CEST). Journal of Magnetic Resonance. 2000;143(1):79-87.

24. McConnell H. Reaction rates by nuclear magnetic resonance. The Journal Of Chemical Physics. 1958;28(3):430-1.

25. van Zijl PCM, Sehgal AA. Proton Chemical Exchange Saturation Transfer (CEST) MRS and MRI. eMagRes, 2016. 5. p. 1307-32.

26. Zhou J, Zijl PCMv. Chemical exchange saturation transfer imaging and spectroscopy. Progress in Nuclear Magnetic Resonance Spectroscopy. 2006;48(2-3):109-36.

27. Zhou J, van Zijl PC. Defining an Acidosis-Based Ischemic Penumbra from pH-Weighted MRI. Translational Stroke Research. 2011;3(1):76-83.

28. Song G, Li C, Luo X, Zhao X, Zhang S, Zhang Y, et al. Evolution of Cerebral Ischemia Assessed by Amide Proton Transfer-Weighted MRI. Frontiers in Neurology. 2017;8:67.

29. van Zijl PCM, Lam WW, Xu J, Knutsson L, Stanisz GJ. Magnetization Transfer Contrast and Chemical Exchange Saturation Transfer MRI. Features and analysis of the field-dependent saturation spectrum. Neuroimage. 2018;168:222-41.

30. Zhou J, Lal B, Wilson DA, Laterra J, van Zijl PC. Amide proton transfer (APT) contrast for imaging of brain tumors. Magn Reson Med. 2003;50(6):1120-6.

31. Ling W, Regatte RR, Navon G, Jerschow A. Assessment of glycosaminoglycan concentration in vivo by chemical exchange-dependent saturation transfer (gagCEST). Proceedings of the National Academy of Sciences. 2008;105(7):2266-70.

32. Singh A, Haris M, Cai K, Kassey VB, Kogan F, Reddy D, et al. Chemical exchange saturation transfer magnetic resonance imaging of human knee cartilage at 3 T and 7 T. Magnetic Resonance in Medicine. 2012;68(2):588-94.

33. Haris M, Nath K, Cai K, Singh A, Crescenzi R, Kogan F, et al. Imaging of glutamate neurotransmitter alterations in Alzheimer's disease. NMR in Biomedicine. 2013;26(4):386-91.

34. Kejia Cai, Mohammad Haris, Anup Singh, Feliks Kogan, Joel H Greenberg, Hari Hariharan, et al. Magnetic resonance imaging of glutamate. Nature Medicine. 2012;18:302-6.

35. Marieb EN, Hoehn K. Human anatomy & physiology 7 ed. San Fransisco: Pearson Education; 2007.

36. Bardet S, Pasqual C, Maugendre D, Remy JP, Charbonnel B, Sai P. Inter and intra individual variability of acute insulin response during intravenous glucose tolerance tests. Diabetes & Metabolism. 1989;15(5):224-32.

37. Mergenthaler P, Lindauer U, Dienel GA, Meisel A. Sugar for the brain: the role of glucose in physiological and pathological brain function. Trends in Neurosciences. 2013 36(10):587-97.

38. Delbeke D, Coleman RE, Guiberteau MJ, Brown ML, Royal HD, Siegel BA, et al. Procedure Guideline for Tumor Imaging with 18F-FDG PET/CT 1.0. The Journal Of Nuclear Medicine. 2006;47(5).

39. Klein S, Staring M, Murphy K, Viergever MA, Pluim JPW. elastix: a toolbox for intensity based medical image registration. IEEE Transactions on Medical Imaging. 2010;29(1):196-205.

40. Xu X, Xu J, Knutsson L, Li Y, Liu H, Liu G, et al. The origins of glucoCEST signal: effect inhibiting glucose transport in brain tumors. Abstract #0186. International Society for Magnetic Resonance in Medicine. Singapore. 2016; May 7-13

41. Knutsson L, Ståhlberg F, Wirestam R. Absolute quantification of perfusion using dynamic susceptibility contrast MRI: pitfalls and possibilities. Magnetic Resonance Materials in Physics, Biology and Medicine. 2010 23(1):1-21.

42. Puri BK, Lewis HJ, Saeed N, Davey NJ. Volumetric change of the lateral ventricles in the human brain following glucose loading. Experimental Physiology. 1999;84:223-6.